Navigating Extremes: River Levels and Grain Transportation System Resilience

Shujie Wu[1], Todd Hubbs[2], Mindy Mallory[3], and Teresa Serra[4]

Acknowledgements*: This research was supported by the Office for Futures and Options Research at the University of Illinois Urbana-Champaign. The authors received no other financial support for this research and have no financial relationships or other potential conflicts of interest relevant to this study to disclose.*

[1] Department of Agricultural and Consumer Economics, University of Illinois Urbana-Champaign, 1301 W Gregory Dr, Urbana, IL 61801, USA. Email: shujiew2@illinois.edu. Corresponding author.

[2] Department of Agricultural Economics, Oklahoma State University, Agricultural Hall, Stillwater, OK 74078, USA. Email: todd.hubbs@okstate.edu.

[3] Department of Agricultural Economics, Purdue University, 615 Mitch Daniels Blvd, West Lafayette, IN 47907, USA. Email: mlmallor@purdue.edu.

[4] Department of Agricultural and Consumer Economics, University of Illinois Urbana-Champaign, 1301 W Gregory Dr, Urbana, IL 61801, USA. Email: tserra@illinois.edu.

Abstract

Extreme fluctuations in Upper Mississippi River water levels threaten the reliability of U.S. grain transportation. We quantify how hydrological extremes transmit through barge logistics to inland-export grain price spreads, transportation costs, and shipment volumes. Using a multi-regime Global Vector Autoregressive model with weekly data (2013-2022), we find that drought-induced low-water conditions coincide with the largest market disruptions. Simulations based on a 15-foot water level drop show corn price spreads widening by up to 41%, barge rates increasing by up to 94%, and shipments declining by 29-40%. While soybean spreads widen even more, shipments remain statistically unchanged, suggesting that soybean transportation is more river-dependent and inelastic. In contrast, flood shocks are associated primarily with shipment disruptions, with more persistent effects for corn, temporary effects for soybeans, and negligible price responses. Results underscore how climate-related transportation disruptions can weaken spatial market integration, increase supply chain vulnerability, and challenge the reliability of U.S. agricultural exports, highlighting the importance of climate adaptation and inland waterway infrastructure resilience for maintaining food system stability and trade competitiveness.

Key Words: Grain barge transportation; Inland-export price spreads; Mississippi river floods and droughts; Multi-regime Global VAR model

JEL Classification: C32, Q11, Q54

Introduction

The United States is a global leader in corn and soybean exports, with production concentrated in the Midwest. In 2022, approximately 17% of U.S. corn and nearly half of soybean production were exported. The Mississippi River system carries roughly half of all U.S. grain exports to the Gulf of Mexico (Henderson et al., 2023). To facilitate this, the U.S. Army Corps of Engineers manages a system of locks and dams designed to maintain a 9-foot navigation channel (Appendix A) north of St. Louis, where navigation depends on lock operations.

Unfavorable Mississippi River system water levels disrupt grain transportation, increase supply chain frictions, weaken spatial price integration, and widen inland-export price spreads. These conditions arise when water levels are either too low to support barge navigation or too high, thereby increasing navigational risk and operational constraints. These disruptions reverberate throughout the grain supply chain and raise concerns regarding food system resilience. For producers, they reduce profit margins while increasing volatility in price spreads, particularly for farms distant from alternative transportation options for export or domestic processing. Grain handlers and river terminals face heightened logistical and storage risks as barge capacity constraints delay shipments and disrupt contracting schedules, often forcing costly shifts to alternative rail or truck transportation. For policymakers, the increasing frequency of hydrological extremes highlights the vulnerability of inland transportation infrastructure to weather-related shocks and underscores the importance of adaptation investments aimed at maintaining stable agricultural trade and food supply systems.

The objective of this study is to quantify how extreme water-level fluctuations in the Upper Mississippi River system transmit through barge transportation costs and capacity constraints to inland–export grain price spreads. While river conditions are a primary driver of logistical frictions, barge transportation is also sensitive to energy prices, which acts as a key cost shifter. Accordingly,

we examine how droughts, floods, and energy cost shocks propagate dynamically and spatially across connected river segments, and whether these transmission mechanisms differ across commodities and market participants. By jointly modeling river hydrology, barge logistics, and regional price spreads within a unified framework, we aim to provide a system-wide assessment of how weather-driven river disruptions affect grain market integration and export reliability.

Previous literature examines how river conditions shape barge transportation costs and navigability along the Mississippi River system. Li (2013a) uses a piecewise linear regression, showing barge rates spike once water levels fall below critical thresholds, while Chen et al. (2024) identify a U-shaped relationship between barge rates and water levels, with both droughts and floods driving rapid rate increases. Other studies emphasize the spatial dimension of transportation disruptions. Chen and Cheng (2024) use a Spatial Durbin Model (SDM) to show that river lock closures significantly raise barge rates and generate regional spillovers across connected river segments. Related transportation studies highlight that both droughts and floods constrain river capacity and disrupt freight movements, with high-water events increasingly fragmenting navigability along the Mississippi River system (Amorim et al., 2023). Quaye et al. (2025) further document interregional spillover effects in barge rate volatility employing a SDM.

Another strand of research links transportation costs to spatial grain price dynamics. Using cointegration analysis, Yu et al. (2007) demonstrate that shocks to barge rates affect export–local price relationships over the long run. Li (2013b) shows that higher barge rates between St. Louis and New Orleans reduce Midwest corn prices relative to Gulf prices. While these studies establish transportation costs as a key driver of inland–export price spreads, they focus on how changes in barge rates transmit to grain prices, without explicitly modeling the river conditions that generate transportation disruptions.

Event-specific studies examine the effects of extreme hydrological events on grain markets. Using the 1993 drought as a case study, McNew (1996) finds that price transmission between inland markets and New Orleans was reduced by roughly one half. Flores and Janzen (2023) show that drought effects decline with distance from the river and proximity to processing facilities. Related studies shift attention from price transmission to quantity and welfare impacts. Steinbach and Zhuang (2025) quantify reductions in agricultural shipments and associated economic losses resulting from the 2022 Mississippi River drought. Mitchell and Biram (2025) estimate the economic costs of the 2022 drought conditions using Arkansas soybean basis data. Evidence on flooding events remains limited, consisting mainly of descriptive reports of shipment disruptions during major flood events, such as the prolonged closure of the St. Louis Harbor during the 2019 flood (Fahie, 2019).

Collectively, existing studies document individual links between river conditions, transportation costs, shipments, and grain market outcomes. However, these mechanisms are typically examined in isolation and lack an integrated empirical framework that captures the dynamic, spatial and regime-dependent transmission of hydrological shocks through barge transportation costs and capacity constraints to inland–export grain price spreads and shipment flows.

We address this gap by developing a multi-regime Global Vector Autoregressive (MR-GVAR) framework that integrates river hydrology, barge transportation outcomes, and regional grain price spreads within a unified, spatially connected system. The model characterizes how water-level fluctuations, ranging from flood to drought, propagate through barge transportation costs and capacity constraints to affect inland–export grain price spreads and shipment flows. The framework simulates and quantifies how river-induced shocks propagate across interconnected

Midwest grain markets over space and time.

To operationalize this framework, we use weekly data from 2013 to 2022, which incorporates St. Louis gauge heights and diesel prices as global variables, alongside regional barge freight rates, shipment volumes, and grain elevator and processor price spreads across three primary river segments: Upper Mississippi – Rock Island segment (UM-RI), Upper Mississippi – St. Louis segment (UM-SL), and Illinois River segment (UM-IL).[5] A shipment-weighted spatial matrix captures interregional connectivity, while a threshold-switching mechanism distinguishes drought, normal, and flood regimes. Using Generalized Impulse Response Functions (GIRFs), we characterize the dynamic relationships between hydrological shocks and regional outcome variables.

Results reveal clear differences in how droughts and floods affect inland grain markets. Drought-induced low-water conditions generate the largest disruptions, with a 15-foot decline in river levels increasing barge rates by up to 94%, widening corn elevator and processor price spreads by up to 41%, and reducing corn shipment volumes by 27–40%. Soybean price spreads widen even more—by up to 61%—yet shipment volumes remain statistically unchanged, suggesting that soybean transportation is more river-dependent and therefore adjusts primarily through prices rather than quantities under low-water conditions. In contrast, flood events primarily disrupt shipment flows, with persistent effects for corn and more temporary effects for soybeans, while generating negligible responses in barge rates and inland–export price spreads.

The framework makes four key contributions. First, we develop a MR-GVAR framework that jointly models river hydrology, barge transportation costs, shipment flows, and regional grain price spreads within a unified, spatially connected system. Unlike previous studies that separately

[5] Rock Island segment contains lock 15 and nearby locks, St. Louis segment includes lock 27 and nearby locks, and Illinois River segment refers to Lock La Grange and surrounding regions. See details in Appendix A.

assess how water levels affect barge rates (Li, 2013b), or how transportation costs influence price spreads (McNew, 1996; Flores & Janzen, 2023), our framework captures their dynamic interactions simultaneously, providing a system-wide representation of grain transportation and market adjustment.

Second, the framework explicitly captures the dynamic and spatial transmission of hydrological shocks across interconnected river segments, allowing us to quantify how local river disruptions propagate through regional grain transportation networks and inland–export grain markets over time. Third, by incorporating diesel prices as an exogenous cost shifter, the framework distinguishes hydrological shocks from concurrent energy-price shocks. Unlike studies of the 2022 drought, where water-level and energy-price shocks coincided, our framework enables a clearer assessment of the independent effects of river conditions on transportation costs, shipment flows, and grain price spreads. Fourth, the multi-regime specification accommodates heterogeneous responses across commodities and hydrological regimes, allowing droughts and floods to differ in both the magnitude and persistence of their effects. This flexibility provides new evidence on the resilience of U.S. inland waterway logistics and offers policy-relevant insights for infrastructure investment, climate adaptation, and maintaining reliable agricultural export supply chains.

Conceptual Framework

Under the Law of One Price, spatial price differentials reflect physical commodity arbitrage costs, with transportation costs playing a central role in linking inland grain markets to export destinations (von Cramon-Taubadel & Goodwin, 2021). In the Mississippi River system, barge transportation constitutes a major component of these costs. Changes in river conditions affect barge freight rates and, consequently, inland-export price spreads and grain shipments by altering

the cost of moving grain between production regions and terminal markets (Yu et al., 2007; Li, 2013b).

Transportation costs are also influenced by energy prices. While water levels affect carrying capacity and navigation efficiency, diesel prices determine a substantial portion of barge operating costs. Incorporating energy costs therefore helps distinguish transportation frictions arising from physical navigation constraints from those driven by broader macroeconomic cost pressures. River stages at key hydrological nodes and diesel prices therefore act as system-wide drivers influencing transportation conditions across connected river segments.

The transmission of river conditions to prices and shipments is state-dependent. Low-water conditions reduce effective channel depth, limiting tow sizes and barge availability through binding draft constraints (McNew, 1996; Li, 2013a; Flores & Janzen, 2023; Chen & Cheng, 2024), whereas high-water conditions primarily introduce episodic navigational risks (Amorim et al., 2023). Droughts are expected to raise freight rates and restrict effective shipping capacity, leading to wider inland-export price spreads and quantity restrictions, while floods are more likely to cause short-lived shipment disruptions. Responses may also differ across commodities as limited transportation capacity is allocated according to market incentives.

Because river segments are connected through shared logistics and contracting relationships, shocks originating at key hydrological nodes can propagate spatially across connected regions over time. In particular, river stages at St. Louis provide a natural system-wide hydrological indicator because navigability conditions at this node strongly influence transportation across interconnected Mississippi and Illinois River networks. Capturing these dynamics requires a framework that jointly models prices, transportation costs, and shipment volumes within a spatially connected system, while allowing the strength and persistence of these

linkages to vary across hydrological regimes. This motivates the MR-GVAR approach adopted in the empirical analysis.

Data and Descriptive Analysis

We use daily corn and soybean spot bids from GeoGrain (via Bloomberg) spanning January 1, 2013, to December 31, 2022, the longest consistently sample across all variables. The dataset includes daily bid prices (dollars per bushel) reported by Midwest grain elevators and processing facilities such as ethanol plants, feed mills, and crushing plants, along with their geographic coordinates. Facilities with more than 15% missing observations are excluded. Daily Gulf Coast elevator bids for corn and soybean are sourced from the USDA Louisiana and Texas Export Bids report and serve as the export market benchmark. Weekly diesel prices (dollars per gallon) are obtained from the U.S. Energy Information Administration to account for fuel-driven variation in barge transportation costs and competing road-freight rates.

Weekly grain barge movements (tons) are obtained from USDA's Downbound Grain Barge Movement report. We focus on shipments measured at three locks representing the primary inland waterway segments in the study: Lock 15 (UM-RI), Lock 27 (UM-SL), and Lock La Grange (UM-IL). Corresponding barge transportation costs are obtained from USDA's Weekly Barge Rates report, which quotes rates as a percentage of the 1976 benchmark tariff and reports rates by river segments. Each barge rate series is matched to the corresponding lock location used in the barge movement data. Daily river levels[6] at St. Louis are collected from the U.S. Geological Survey. The St. Louis gauge is the primary hydrological indicator because water levels at this location largely govern navigability across the interconnected Mississippi–Illinois river system.

[6] They represent the water surface elevation relative to a fixed vertical datum above sea level (NAVD88). See https://waterdata.usgs.gov/nwis/dv?referred_module=sw&site_no=07010000.

To harmonize data and reduce daily noise, all variables are aggregated to weekly averages, except barge movements, which are weekly totals. Missing daily grain prices are imputed using the most recent available observation to address short reporting gaps. Barge movement data are not imputed, because zero observations reflect actual periods of limited or suspended navigation. Missing barge rates are also filled using the last available quotation because reported rates are unavailable during severe navigation disruptions, when barge transactions become too limited to generate observable market prices. This procedure is expected to attenuate the estimated barge rate responses during extreme hydrological events. Hence, the estimated barge-rate effects should be interpreted as conservative measures of transportation disruption costs.

We calculate inland–export price spreads as the difference between each elevator and processor spot bids and Gulf export bids. By construction, a negative spread reflects positive transaction costs of moving grain from inland origins to export markets. To strengthen the linkage between river conditions and local price formation, we restrict our sample to elevators within a 50-mile radius of the inland waterway system, following Sytsma and Wilson (2021), who show that facilities within this proximity strongly prefer barge transportation. Each elevator is assigned to its nearest benchmark port within 50 miles, mapping facilities to one of the three MR-GVAR transportation regions. As a robustness check, we later expand the assignment radius to 100 miles.

Processors, representing domestic grain demand, are also matched to elevators based on geographic proximity: each elevator is paired with its nearest processor within 50 miles. Regional elevator and processor price spreads are then calculated by averaging facility-level price spreads within each barge transportation region. These regional averages constitute the inland price variables used in the empirical analysis. Figures B1 and B2 in Appendix B show the distribution of corn and soybean elevators and processors.

Seasonal navigation constraints significantly impact barge transportation on the Upper Mississippi River. During winter months, freezing conditions can lead to partial or complete shutdowns of upstream lock operations. Figures B3 and B4 in Appendix B show a pronounced collapse in barge movements during January and February across the locks, especially in the UM-RI segment. Because these months reflect severe winter navigation constraints rather than normal shipping activities, we exclude January and February from the main sample and later reintroduce them as a robustness check

After excluding winter months, barge movements and river stages still exhibit distinct seasonal patterns. As shown in Figures B3 and B4 in Appendix B, corn shipments tend to concentrate during relatively higher water levels, while soybean movements peak in the fall when river stages are lower, indicating that shipping seasonality is market-driven rather than purely hydrologically determined. To ensure that estimated relationships capture deviations from typical seasonal behavior rather than recurring market cycles, we deseasonalize all endogenous variables. Specifically, we use dummy-variable regressions with monthly indicators and use the residuals in the analysis (see details in Methods and Empirical Approach).

Table 1 reports the summary statistics for the 442 weekly observations spanning the study period. Panel A presents global variables, with median river levels at 15.02 feet and diesel prices at $3.01 per gallon. Both variables exhibit substantial variation, reflecting periods of hydrological stress and energy price volatility. Panels B and C report regional weekly elevator and processor price spreads, barge rates, and barge movements for corn and soybeans across the UM-RI, UM-SL, and UM-IL. For both commodities and across all regions, median elevator and processor price spreads are negative, consistent with positive transactions costs associated with moving grain from inland origins to export terminals. This is most pronounced in the UM-RI, where median elevator

spreads are -74.39 and -93.01 cents per bushel for corn and soybeans respectively. Barge rates demonstrate extreme right-skewness; while medians hover between 300% and 406.75%, maximum values exceed 2,000% during severe logistical disruption. Shipment volumes also vary substantially across regions. UM-SL functions as the primary transit corridor, with median corn and soybean movements far exceeding those in UM-RI and UM-IL. While these statistics describe raw data, all estimation and impulse response analyses use deseasonalized variables to isolate idiosyncratic shocks from predictable seasonal patterns.

Table 2 categorizes the sample into drought, normal, and flood regimes based on river stages at St. Louis. The drought and flood regimes are defined using fixed river-stage thresholds at the St. Louis gauge corresponding to operational navigation benchmarks (see Methods and Empirical Approach Section). While the normal regime accounts for most observations, the sample includes 135 drought and 49 flood weeks, providing sufficient variation to estimate regime-dependent dynamics and implement the stratified bootstrap procedure employed in our simulation analysis.

The Upper Mississippi River system experienced several episodes of extreme hydrological stress during the sample period. Two events are especially prominent. In late May 2019, St. Louis river stages exceeded 40 feet, reaching major flood conditions and leading to widespread lock closures. In contrast, the 2022 drought generated prolonged low water conditions, with river stages falling below the zero-gage datum for multiple consecutive weeks. This event severely constrained channel capacity and barge operations, generating pronounced disruptions to grain transportation.

Figures 1-3 illustrate UM–SL price spreads, barge movements, and barge rates alongside St. Louis river stages, with corresponding regional plots reported in Appendix B. The data reveal a nonlinear relationship between river conditions and market outcomes. Price spreads and barge

rates remain relatively stable under moderate river stages but widen sharply during extreme low-water periods, especially during the 2022 drought. High-water events elicit more muted and transitory responses, suggesting that flood-related frictions are less binding than the low-water bottlenecks. Under extreme low-water conditions, rising barge rates acts as a transportation-cost 'wedge' that weakens regional grain price integration.

Figure 2 plots corn and soybean shipments for UM–SL over time, visually confirming the distinct seasonal patterns discussed above. Soybean shipments concentrate after harvest, while corn shipments extend into the spring and summer months when the river levels are more favorable. This persistence underscores the importance of deseasonalizing the variables before examining the relationship between hydrologic conditions and price spreads, as seasonal shipment behavior could otherwise confound hydrology-driven effects.

Figures B5–B9 in Appendix B show highly synchronized responses in price spreads, barge rates, and shipment volumes across the three regions during extreme events, indicating system-wide transportation disruptions. However, the magnitude and persistence of responses vary across regions, suggesting heterogeneous exposure to river constraints.

Method and Empirical Approach

Treatment of Seasonal Trends

To isolate idiosyncratic shocks from recurring seasonal patterns in grain prices and transportation variables, we deseasonalize each endogenous variable using a monthly dummy-variable regression:

$$y_{i,t} = D_t\delta_i + u_{i,t}, \quad (1)$$

where D_t is a vector of monthly indicators D_{mt} equaling 1 if observation t falls in month m, and 0 otherwise. The deseasonalized series is defined as the regression residuals, $y_{i,t}^{ds} = u_{i,t}$. This procedure removes deterministic monthly effects while preserving regime-dependent dynamics or

shock transmission.

The baseline GVAR model

Building on the descriptive evidence, we adopt a GVAR framework (Pesaran et al., 2004, Dees et al., 2007, and Chudik & Pesaran, 2016) to model dynamic interactions among river conditions, barge transportation outcomes, and regional grain price spreads. The GVAR captures cross-regional linkages while preserving region-specific dynamics, making it well suited to the interconnected Mississippi River system.

Let i index N regions and $t = 1, \ldots, T$ denote time. For each region, the $k \times 1$ vector of region-specific deseasonalized endogenous variables is defined as:

$$y_{i,t}^{ds} = \begin{bmatrix} Elevator\ Spread_{i,t}^{ds} \\ Processor\ spread_{i,t}^{ds} \\ Barge\ Rate_{i,t}^{ds} \\ Barge\ Movement_{i,t}^{ds} \end{bmatrix}. \quad (2)$$

The $n \times 1$ vector of global exogenous variables is defined as:

$$x_t = \begin{bmatrix} Water\ level_t \\ Diesel\ price_t \end{bmatrix}. \quad (3)$$

The baseline region-specific GVAR model is:

$$y_{i,t}^{ds} = a_i + \Phi_i y_{i,t-1}^{ds} + \Lambda_i y^{ds^*}_{i,t} + \Gamma_i y^{ds^*}_{i,t-1} + \beta_i x_t + \varepsilon_{i,t},\ \varepsilon_{i,t} \sim iid(0, \Sigma_{ii}), \quad (4)$$

where a_i is a $k \times 1$ vector of region-specific intercepts; Φ_i is a $k \times k$ matrix of coefficients capturing own-region lagged effects; $y^{ds^*}_{i,t}$ and $y^{ds^*}_{i,t-1}$ are $k \times 1$ vectors of contemporaneous and lagged foreign variables, constructed as weighted averages of endogenous variables from the other regions; Λ_i and Γ_i are $k \times k$ coefficient matrices capturing cross-regional spillover effects; β_i is the $k \times n$ matrix of global variable coefficients; and Σ_{ii} denotes the covariance matrix of region-specific innovations.

To capture the specific channel through which hydrological shocks transmit to grain markets, we impose economically motivated exclusion restrictions on β_i. We exclude water levels from the price-spread equations, reflecting the spatial arbitrage assumption that river conditions affect grain prices indirectly through transportation costs and capacity constraints, rather than a direct pricing channel. Water levels therefore enter only the barge rate and movement equations. Diesel prices are allowed to enter all equations without restriction, as fuel costs influence not only barge rates, but also the cost of competing transportation modes such as rail and truck transportation. As a result, energy price fluctuations may affect transportation costs, shipment decisions, and inland–export price spreads simultaneously. The restricted global variable coefficient matrix is:

$$\beta_i = \begin{bmatrix} 0 & \beta_{ES}^{DP} \\ 0 & \beta_{PS}^{DP} \\ \beta_{BR}^{WL} & \beta_{BR}^{DP} \\ \beta_{BM}^{WL} & \beta_{BM}^{DP} \end{bmatrix} \tag{5}$$

Multi-Regime GVAR Specification

Building on the baseline GVAR framework, we extend the model to a Multi-Regime GVAR (MR-GVAR) specification to capture potential nonlinear responses to river conditions. Following Chen & Semmler (2018), we classify hydrological conditions using two critical benchmarks from the St Louis NOAA river gauge[7] defining three distinct regimes (r_t): a drought regime ($Water\ level_t \leq 9ft$), representing the minimum depth for unrestricted navigation; a flood regime ($Water\ level_t > 28$ft), representing the stage at which mitigation activities are initiated; and a normal regime ($9ft < Water\ level_t \leq 28ft$). The regime indicator is:

[7] Mississippi River at St. Louis: https://water.noaa.gov/gauges/eadm7

$$r_t = \begin{cases} 1, & Water\ level_t \leq 9ft \\ 2, & 9ft < Water\ level_t \leq 28ft. \\ 3, & Water\ level_t > 28ft \end{cases} \quad (6)$$

The regime thresholds are fixed ex ante using institutional navigation and flood-stage benchmarks at the St. Louis gauge, rather than estimated endogenously. A river stage of 9 feet corresponds to the minimum depth required for unrestricted barge navigation, while 28 feet marks the onset of flood-stage management and navigation restrictions. Using externally defined thresholds avoids data-driven regime selection and anchors the regimes to physical constraints on river operations.

Conditional on regime r_t, the MR-GVAR region *i* is given by:

$$y_{i,t}^{ds} = a_i^{(r_t)} + \Phi_i^{(r_t)} y_{i,t-1}^{ds} + \Lambda_i^{(r_t)} y^{ds^*}_{i,t} + \Gamma_i^{(r_t)} y^{ds^*}_{i,t-1} + \beta_i^{(r_t)} x_t + \varepsilon_{i,t}^{(r_t)}, \ \ \varepsilon_{i,t}^{(r_t)} \sim iid(0, \Sigma_{ii}^{(r_t)}) \quad (7)$$

All model coefficients and covariance matrices are vary across regimes, capturing regime-specific differences in dynamic adjustments, cross-regional spillovers, and shock transmission. The regime indicator r_t is common across regions, reflecting the integrated nature of the Mississippi River system, where extreme water levels constitute a system-wide logistical shock that simultaneously affects connected river segments.

The weight matrix

Foreign variables are constructed using a region-specific spatial weight matrix based on cumulative barge grain flows through each river port aggregated over the full sample period. This shipment-based weighting scheme captures long-run transportation connectivity across the river network rather than short-run fluctuations. Formally, for each region *i*, the *k*×1 vector of foreign variables is defined as:

$$y^{ds^*}_{i,t} = \sum_{j \neq i} w_{ij} y_{j,t}^{ds}, \quad (8)$$

where w_{ij} denotes the spatial weight assigned to region *j*. Each off-diagonal element w_{ij} is defined as the share of cumulative barge grain quantities passing through port *j* relative to the total

cumulative barge grain quantities associated with region i. Diagonal elements are set to zero so that a region's foreign variables exclude its own endogenous outcomes, and weights sum to one across other regions. Cumulative flows reduce the influence of short-run weekly movement variations, which are already modeled as endogenous variables. With a fixed weight matrix, cross-regional transmission is reflected in the estimated model coefficients rather than time-varying weights.

Parameter estimation

The exclusion restrictions imposed on β_i create equations with different sets of explanatory variables. In this unbalanced system, Seemingly Unrelated Regression (SUR) provides more efficient parameter estimates by accounting for the contemporaneous correlation across equation errors (Zellner, 1962). However, our system is high-dimensional and unbalanced, causing the estimated error covariance matrix to become ill-conditioned, and producing unstable SUR estimates. We therefore estimate each regional equation separately using OLS, which delivers numerically stable and consistent parameter estimates while preserving the region-specific structure of the model.

The Solution of the MR-GVAR

After estimating each region-specific model, we construct the global coefficient matrices. First, we define the (k+k) × 1 vector $z_{i,t}$ as:

$$z_{i,t} = \begin{bmatrix} y_{i,t}^{ds} \\ y_{i,t}^{ds*} \end{bmatrix}, \tag{9}$$

This allows us to rewrite the regional model from equation (7) in a more compact form:

$$A_i^{(r_t)} z_{i,t} = a_i^{(r_t)} + B_i^{(r_t)} z_{i,t-1} + \beta_i^{(r_t)} x_t + \varepsilon_{i,t}^{(r_t)}, \tag{10}$$

in which

$A_i^{(r_t)} = [I_k, -\Lambda_i^{(r_t)}]$ and $B_i^{(r_t)} = [\Phi_i^{(r_t)}, \Gamma_i^{(r_t)}]$

Both $A_i^{(r_t)}$ and $B_i^{(r_t)}$ are $k \times (k+k)$ matrices. We define a $(k+k) \times Nk$ constant matrices W_i (for i=0,1,2) constructed from the time-invariant weights, such that

$$z_{i,t} = W_i y_{i,t}^{ds} , \tag{11}$$

where $W_0 = \begin{bmatrix} I_4 & 0 & 0 \\ 0 & w_{01}I_4 & w_{02}I_4 \end{bmatrix}$, $W_1 = \begin{bmatrix} 0 & I_4 & 0 \\ w_{10}I_4 & 0 & w_{12}I_4 \end{bmatrix}$, and $W_2 = \begin{bmatrix} 0 & 0 & I_4 \\ w_{20}I_4 & w_{21}I_4 & 0 \end{bmatrix}$.

Substituting (11) in (10) yields:

$$A_i^{(r_t)} W_i \boldsymbol{y}_t = a_i^{(r_t)} + B_i^{(r_t)} W_i \boldsymbol{y}_{t-1} + \beta_i^{(r_t)} x_t + \varepsilon_{i,t}^{(r_t)} , \tag{12}$$

where $\boldsymbol{y}_t = \begin{bmatrix} y_{0,t}^{ds} \\ y_{1,t}^{ds} \\ y_{2,t}^{ds} \end{bmatrix}$.

Stacking regional equations together yields:

$$G^{(r_t)} \boldsymbol{y}_t = a^{(r_t)} + H^{(r_t)} \boldsymbol{y}_{t-1} + \Psi^{(r_t)} x_t + \varepsilon_t^{(r_t)} , \tag{13}$$

where $G^{(r_t)} = \begin{bmatrix} A_0^{(r_t)} W_0 \\ A_1^{(r_t)} W_1 \\ A_2^{(r_t)} W_2 \end{bmatrix}$, $H^{(r_t)} = \begin{bmatrix} B_0^{(r_t)} W_0 \\ B_1^{(r_t)} W_1 \\ B_2^{(r_t)} W_2 \end{bmatrix}$, $a^{(r_t)} = \begin{bmatrix} a_0^{(r_t)} \\ a_1^{(r_t)} \\ a_2^{(r_t)} \end{bmatrix}$, $\Psi^{(r_t)} = \begin{bmatrix} \beta_0^{(r_t)} \\ \beta_1^{(r_t)} \\ \beta_2^{(r_t)} \end{bmatrix}$, and $\varepsilon_t^{(r_t)} = \begin{bmatrix} \varepsilon_{0,t}^{(r_t)} \\ \varepsilon_{1,t}^{(r_t)} \\ \varepsilon_{2,t}^{(r_t)} \end{bmatrix}$.

Provided that $G^{(r_t)}$ is nonsingular, the reduced form of the system is represented by:

$$\boldsymbol{y}_t = G^{-1(r_t)} a^{(r_t)} + G^{-1(r_t)} H^{(r_t)} \boldsymbol{y}_{t-1} + G^{-1(r_t)} \Psi^{(r_t)} x_t + G^{-1(r_t)} \varepsilon_t^{(r_t)} . \tag{14}$$

Let $F^{(r_t)} = G^{-1(r_t)} H^{(r_t)}$. The stability of the global system is assessed separately for each hydrological regime. The system is stable in regime (r_t) if all eigenvalues of the regime-specific transition matrix $F^{(r_t)}$ lie strictly inside the unit circle. This condition ensures that shocks dissipate over time and that the dynamic responses are well defined.

Weak Exogeneity Assumption

In standard GVAR models, foreign variables can be treated as weakly exogenous when the cross-

sectional dimension of the system (*N*) is sufficiently large, such that the individual weights are small ($w_{01} \to 0$ as $N \to \infty$) (Pesaran et al. 2004). Under this assumption, feedback from any individual region to the foreign aggregates is asymptotically negligible. However, this assumption is unlikely to hold in our setting, which contains only three interconnected river regions. Shocks in one region, such as the Illinois River segment, may have a non-negligible effect on the foreign aggregates of neighboring regions. Treating foreign variables as weakly exogenous could therefore bias inference.

We address this concern by adopting a conditional MR-GVAR approach (Pesaran et al. 2004, and Dees et al. 2007) appropriate for systems with a dominant unit or small cross-sections. Rather than imposing weak exogeneity, we allow simultaneity between region-specific endogenous variables $y_{i,t}^{ds}$ and their corresponding foreign aggregates $y_{i,t}^{ds*}$, and treat foreign variables as endogenous. The estimated coefficients and covariance matrices from the joint system are used to construct the conditional model $y_{i,t}^{ds}|y_{i,t}^{ds*}$, which serves as the baseline for the simulations and GIRF analysis. Appendix C provides the technical derivation.

Shock Simulation and Bootstrap Inferences

Based on the reduced-form MR-GVAR representation, we conduct counterfactual simulations to examine how extreme hydrological and energy cost shocks propagate through barge transportation and regional grain price spreads. Simulations are performed conditional on each hydrological regime, using regime-specific coefficient matrices and covariance matrices computed from the regime-specific residuals.

We consider three shock scenarios, each implemented as a 20-week deterministic path where the shocked variable is held fixed while other exogenous variables remain at their sample medians. First, a drought scenario reduces the St. Louis river stage from its sample median to 0

feet. Second, a flood scenario increases the river stage from the sample median to 40 feet. The two scenarios represent binding navigation constraints and elevated flood risk, respectively. Third, an energy cost scenario raises the diesel price from its sample median to $5 per gallon, reflecting sharp increases in fuel costs. The 20-week horizon allows the effects of each shock to evolve and permits regime transitions during the simulation. By imposing sustained deviations in key exogenous variables, the simulations trace the dynamic adjustment outcomes of barge transportation and regional grain price spreads under prolonged stress.

Unlike conventional impulse response analysis, which introduces shocks as one-time innovations to the reduced-form residuals, we implement shocks by directly altering the exogenous variable levels. This approach is appropriate because river levels and diesel prices are modeled as exogenous common drivers rather than endogenous stochastic processes. In addition, severe floods and droughts are tail events that are not well approximated by small, transitory innovations around the mean. Imposing large level shifts also allows the system to transition across regimes, which is essential for capturing the regime-dependent nonlinearities of the MR-GVAR framework without relying on full structural identification of the underlying innovations.

Uncertainty surrounding the simulated responses is assessed using a stratified residual bootstrap procedure (Alessio et al. 2025). Residuals are drawn with replacement from regime-specific residual pools, preserving the dependence structure and volatility associated with each regime. For each counterfactual scenario we perform 1,000 bootstrap replications and construct pointwise confidence intervals from the resulting empirical distribution. Following the logic of Dees et al. (2007), but departing from their use of the mean, we report the median of the bootstrap distribution as our central estimate, along with the corresponding confidence bands. This choice provides a robust measure of central tendency in the presence of skewed or heavy-tailed

distributions.

Results

Cointegration test

We examine the long-run relationships among price spreads, barge rates and barge movements. Johansen (1988, 1991) cointegration tests, reported in Table D1 in Appendix D, reject the null hypothesis of no cointegration for all regions and commodities, with an estimated rank of four, the corresponding to the number of endogenous variables. This implies the stationarity of the model variables. Hence, a VAR specification in levels provides an appropriate representation of the joint dynamics.

We do not report the full set of estimated MR-GVAR coefficients because they capture only partial and highly interdependent effects within the system. Dynamic VAR-based models are more informatively interpreted through impulse response analysis. Hence, we focus on regime-dependent GIRFs to characterize the dynamic transmission of hydrological and energy shocks through barge transportation and regional grain price spreads.

Drought

We begin by examining the effects of extreme low-water conditions on inland–export price transmission and barge transportation dynamics. Figure 4 presents the GIRFs of regional corn price spreads and barge transportation variables following a persistent 15-foot decline in the St. Louis water level, from its median level to 0 feet. Shaded areas denote 95% confidence intervals. Across all regions, the drought shock is associated with a significant widening of both elevator and processor price spreads. Most adjustments occur within the first 5-10 weeks, after which responses stabilize and persist, indicating sustained market disruption. Price spreads widen by approximately 20-25 cents per bushel, with the largest responses observed in the UM-SL segment. Relative to

median baseline spreads of roughly -60 to -75 cents per bushel, these changes correspond to a persistent widening of about 27% to 41%, consistent with weaker spatial market integration under low-water conditions.

The disruption in barge transportation mirrors spread responses. Barge rates increase significantly across all regions, rising most sharply within the first 5-10 weeks before stabilizing at around 200% in upstream regions and 280% in UM-SL. Relative to median barge rates of about 400% upstream and 300% downstream, this represents a 50% to 94% increase in transportation costs. Barge movements decline sharply as low water impedes navigation. Upstream movements decline by approximately 25–30 thousand tons, or 29–40% relative to median weekly volumes. UM-SL movements drop by 75 thousand tons, representing about 27% of median weekly volume.

Figure 5 reports GIRFs of regional soybean price spreads and barge transportation variables under the same drought shock. Like corn, drought is associated with a widespread widening of both elevator and processor price spreads. Responses occur quickly in the first 5-10 weeks before stabilizing at approximately 15-20 cents per bushel in UM-SL and 30 cents per bushel in upstream regions, representing around 25-46% of regional median baseline spreads. Relative to corn, soybean elevator spreads exhibit larger absolute changes. This pattern is consistent with soybeans' stronger reliance on export pricing and elevators' role as spatial arbitrage points.

While drought-induced barge rate increases for soybeans are nearly identical to those observed for corn, reflecting the non-commodity-specific nature of barge freight rates, shipment responses differ. Unlike corn, soybean movements do not decline. Median estimates suggest a modest increase, though confidence intervals overlap zero. This stability may reflect soybeans' greater dependence on river-based export channels, with transportation constraints being absorbed primarily through price rather than quantity adjustments.

Overall, drought-induced low-water shocks transmit through both transportation cost and shipment quantity channels, with binding navigation constraints amplifying price adjustments and shipment contractions.

Flood

Figures 6 and 7 show that flood-induced shocks are primarily associated with shipment quantity responses rather than price or transportation cost responses. Shifting the St. Louis water level from 15 to 40 feet is not associated with statistically significant responses in elevator spreads, processor spreads, or barge rates. Instead, the main effects occur through shipment flows. Corn shipments decline, with the largest reductions observed in UM-SL , approximately 100% of median baseline. Soybean shipments decline significantly only in the initial periods following the shock, after which responses gradually recover and become statistically indistinguishable from zero. This divergence highlights commodity-specific adjustment mechanisms. Floods temporarily constrain navigation for both commodities, but corn shipments exhibit more persistent reductions, whereas soybean shipment display greater resilience.

This pattern reflects the transient nature of flood-induced disruptions and differences in commodity exposure to export demand. Flood episodes in the sample are relatively rare and short-lived limiting statistical support for persistent price responses. In addition, the record 2019 flood caused widespread lock closures that suspended both barge movements and barge rate reporting. Because missing barge rates during this period are replaced with the last available observation, estimated cost responses may be attenuated. Shipment responses therefore provide a more reliable indicator for interpreting flood impacts.

Energy

Figures 8 and 9 present GIRFs to an energy-induced shock with diesel price increasing from about

$3 per gallon to $5 per gallon, a 67% increase. This scenario distinguishes energy related increases in transportation costs from hydrology-driven disruptions, which coincided during the 2022 low-water episode. Energy shocks generate more precisely estimated responses along cost-related dimensions, reflected in narrower confidence intervals. Barge rates increase sharply by approximately 37-60% relative to median baseline levels and remain elevated across all regions for both corn and soybean.

These cost pressures are transmitted to grain prices. Elevator spreads widen persistently by about 15 cents per bushel for corn, corresponding to 20-25% of median baseline spreads, and by 20-30 cents per bushel for soybeans, a 21-50% of the median baseline. The larger soybean response is consistent with stronger dependence on export market conditions. Shipment volumes also decline following an energy shock. Declines are especially large in the UM-SL area, where corn and soybean shipments decline by about 54% and 33%, compared to the median level, consistent with prioritization of export-oriented soybean shipments during periods of elevated transportation costs.

Our results align with and extend existing literature by providing a system-wide dynamic analysis of river conditions, barge transportation, and inland grain price transmission. Similar to Li (2013a) and Chen et al. (2024), we observe pronounced nonlinear responses of barge rates to water-level fluctuations, particularly during drought. However, our multi-regime approach extends Yu et al. (2007) and Li (2013b) by embedding hydrological conditions explicitly within the transportation-price transmission framework rather than treating transportation costs as exogenous.

Our findings also extend regime-based analyses of extreme events. While McNew (1996) documented that price transmission during the 1993 drought weakened by roughly one-half, we provide a more granular, dynamic quantification across regions and commodities. Specifically, a

15-foot water level decline is associated with increases in corn and soybean spreads of up to 41% and 46%, respectively. These results complement Flores and Janzen (2023) and Mitchell and Biram (2025) by separating hydrological shocks from concurrent energy-driven cost pressures. Beyond prices, our analysis quantifies the transportation impacts more precisely than previous qualitative or event-based studies. We find that extreme low-water shocks are associated with barge-rate increases of up to 94%. Additionally, while Steinbach and Zhuang (2025) quantified the general reduction in agricultural shipments during the 2022 drought, our study documents heterogeneous commodity responses. Corn shipments contract by 29–40%, whereas soybean shipment volumes remain comparatively stable. This distinction is absent in prior studies and is consistent with the stronger dependence of soybean exports on river transportation under severe transportation constraints.

Robustness Checks

We assess the sensitivity of the MR-GVAR results to sample construction and variable treatment. Excluding January–February observations may disrupt the time-series structure underlying dynamic interregional price transmission. This period is characterized by absent barge activity in the upstream segments, especially UM-RI, and by low water levels. During these winter navigation shutdowns, barge movements are observed as zero, while barge rate quotes are often unreported and imputed using the last available observation. To assess whether excluding winter months affects the estimated dynamics, we conduct two robustness checks: (i) retaining winter months and imputing missing transportation variables, and (ii) retaining winter months while excluding UM–RI, which exhibits no winter barge activity. Results are reported in Appendix E. The first approach leads to a decline in the estimated price impacts under drought, whereas the second yields only moderately smaller effects. This contrast suggests that the reduction in estimated impacts primarily

reflects attenuation from imputing transportation variables during periods of structural non-integration, rather than from excluding winter months.

A 50-mile radius yields a conservative sample of elevators with direct access to barge transportation. We conduct a robustness check that expands the radius to 100 miles, increasing coverage while preserving the spatial mapping to benchmark ports and transportation regions. Results are reported in Appendix F. The resulting impulse responses exhibit only minor differences in magnitude and precision, and the main qualitative conclusions remain unchanged.

Conclusion

We examine the relationship between water level conditions in the Upper Mississippi River system, barge transportation networks, and regional grain markets. Using a multi-regime Global Vector Autoregressive (MR-GVAR) framework linking river stages, energy costs, barge rates and movements, and inland-export elevator and processor price spreads across connected river segments, we show that hydrological and energy-related disruptions are associated with substantial and heterogeneous impacts across commodities and regions.

Two findings emerge. First, drought-induced low-water conditions are associated with the most severe and persistent disruptions. A 15-foot drop in St. Louis river levels is related to an increase in barge transportation costs by 50-94% relative to median levels, wider corn elevator and processor spreads by up to 41% and 61%, and lower corn shipment volumes by 29-40% in upstream regions and 27% in the UM-SL. For soybeans, the transmission mechanism differs. While spreads increase by 25-46% of median values, soybean shipments show no statistically significant decline, consistent with stronger export dependence and differential shipment adjustment for soybeans under transportation constraints.

Second, flood shocks are primarily associated with quantity adjustments rather than

sustained price or cost pressures. While major floods reduce shipments, especially for corn, the effects on spreads and barge rates are comparatively muted and short-lived, consistent with the episodic nature of flood-related navigation interruptions observed in the sample.

These findings highlight the growing vulnerability of food and agricultural supply chains to weather-driven transportation disruptions. First, the pronounced and persistent effects of drought highlight the critical role of channel depth in sustaining navigation reliability. Investments in dredging and sediment management, particularly in drought-prone segments of the Mississippi River, may help alleviate capacity constraints and reduce the transportation shocks to the grain supply chain. Maintaining navigable depths is especially important given the increasing frequency of low-water episodes. Second, the results underscore the importance of lock infrastructure reliability. Aging locks and dams along the Upper Mississippi and Illinois River systems may increase the vulnerability of barge transportation to both low and high water extremes. Improving lock resilience therefore supports both operational continuity and market stability along the entire export corridor.

Beyond hydrological conditions, the results highlight the sensitivity of inland grain transportation to energy cost fluctuations. Because diesel prices affect both barge operating expenses and competing freight modes, elevated fuel costs may amplify transportation frictions even without extreme river conditions. This underscores the importance of considering energy-market volatility alongside physical infrastructure resilience when evaluating inland grain transportation reliability

Finally, the heterogeneous responses of corn and soybean markets suggest that infrastructure investments yield different benefits across commodities. While both crops depend on barge transportation, soybeans' greater exposure to export demand is associated with stronger

basis sensitivity and greater stability in quantity responses. Policy efforts to strengthen inland waterway infrastructure may therefore play a stronger role in preserving soybean spatial price integration and safeguarding the reliability of U.S. grain exports under increasing weather and energy-related risks. Two limitations motivate future work. Flood analysis is constrained by the rarity of severe events and by data gaps during major closures, which may attenuate estimated cost responses. In addition, incorporating rail substitution would further refine the policy implications of river disruptions. Even with these limitations, the MR-GVAR results are consistent with weather-driven river constraints, especially drought-induced low water, posing a material and persistent threat to inland market integration and U.S. export reliability.

References

Alessio, B., Andrea, M., Annamaria, G., & Giuseppe, E. (2025). Spatial bootstrapping using deep clustering methods: Spatial machine learning applied to Lombardy high-tech businesses. *Regional Science Policy & Practice*, 100242. https://doi.org/10.1016/j.rspp.2025.100242

Amorim, R., Villarini, G., Veacth, W., & White, K. (2023). Reduced and more fragmented Mississippi River navigability by rising flow. *Geophysical Research Letters*, *50*(19), e2023GL104619. https://doi.org/10.1029/2023GL104619

Chen, P., & Semmler, W. (2018). Financial stress, regime switching and spillover effects: Evidence from a multi-regime global VAR model. *Journal of Economic Dynamics and Control*, *91*, 318-348. https://doi.org/10.1016/j.jedc.2018.03.001.

Chen, Z., & Cheng, J. (2024). Economic consequences of inland waterway disruptions in the Upper Mississippi River region in a changing climate. *The Annals of Regional Science*, *73*(2), 757–794. https://doi.org/10.1007/s00168-024-01283-0

Chen, Z., Li, Z., & Cheng, J. (2024). The nonlinear impact of climate change on inland waterway transportation in the Upper Mississippi—Illinois River region. *Environmental Research: Infrastructure and Sustainability*, *4*(3), 031001. https://doi.org/10.1088/2634-4505/ad5bfc

Chudik, A., & Pesaran, M. H. (2016). Theory and practice of GVAR modelling. *Journal of Economic Surveys*, *30*(1), 165-197. https://doi.org/10.1111/joes.12095

Dees, S., Mauro, F. D., Pesaran, M. H., & Smith, L. V. (2007). Exploring the international linkages of the euro area: a global VAR analysis. *Journal of Applied Econometrics*, *22*(1), 1-38. https://doi.org/10.1002/jae.932

Fahie, M. (2019). *Impacts of the 2019 upper Mississippi River flooding on barge movements in the upper Midwest region.* United States Coast Guard. https://www.dco.uscg.mil/Portals/9/Impacts%20of%202019%20UMR%20Flooding_Barge%20Movements_Fahie_1.pdf

Flores, I., & Janzen, J. (2023). Low water on the big river: The role of physical and economic distance in US soybean markets, Working Paper, Department of Agricultural and Consumer Economics, University of Illinois Urbana Champaign. https://drive.google.com/file/d/1jcVVHtmcHU9_YSd6YEIszCRFYIqplJvz/view?pli=1

Henderson, R., Caffarelli, P., & Gastelle, J. (2023). *Transportation of U.S. Grains: A Modal Share Analysis 1978 - 2020 Update*. U.S. Department of Agriculture, Agricultural Marketing Service. https://doi.org/10.9752/ts049.08-2023

Johansen, S. (1988), Statistical Analysis of Cointegration Vectors, *Journal of Economic Dynamics and Control*, 12, 231–254. https://doi.org/10.1016/0165-1889(88)90041-3

Johansen, S. (1991), Estimation and Hypothesis Testing of Cointegration Vectors in Gaussian

Vector Autoregressive Models, *Econometrica*, Vol. 59, No. 6, 1551–1580. https://doi.org/10.2307/2938278

Li, S. (2013a). *Water Levels on the Mississippi River and Grain Transport Barge Rates.* [Doctoral dissertation, North Carolina State University]. https://repository.lib.ncsu.edu/server/api/core/bitstreams/5ca3d93c-8eb6-4057-9e77-bef1365889cf/content

Li, S. (2013b). *Grain Transport on the Mississippi River and Spatial Corn Basis*. [Doctoral dissertation, North Carolina State University]. https://repository.lib.ncsu.edu/server/api/core/bitstreams/5ca3d93c-8eb6-4057-9e77-bef1365889cf/content

McNew, K. (1996). Spatial market integration: Definition, theory, and evidence. *Agricultural and Resource Economics Review*, *25*(1), 1–11. https://doi.org/10.1017/s1068280500000010

Mitchell, J. L., & Biram, H. D. (2025). The effects of extreme weather on rural transportation infrastructure and crop prices along the Lower Mississippi River. Applied Economic Perspectives and Policy, 47(3), 1139–1161. https://doi.org/10.1002/aepp.13511

Pesaran, M. H., Schuermann, T., & Weiner, S. M. (2004). Modeling Regional Interdependencies Using a Global Error-Correcting Macroeconometric Model. *Journal of Business & Economic Statistics*, *22*(2), 129–162. http://www.jstor.org/stable/1392171

Quaye, L.-A. A., Stewart, S., & Massa, O. I. (2025). Transportation Disruptions and Corn Basis Volatility along the Mississippi River. Working Paper https://doi.org/10.22004/AG.ECON.361205

Steinbach, S., & Zhuang, X. (2025). US agricultural exports and the 2022 Mississippi River Drought. *Agribusiness*. https://doi.org/10.1002/agr.21880

Sytsma, T., & Wilson, W. (2021). Estimating the Demand for Railroad and Barge Movements of Corn in the Upper Mississippi River Valley. 10.22004/ag.econ.310903

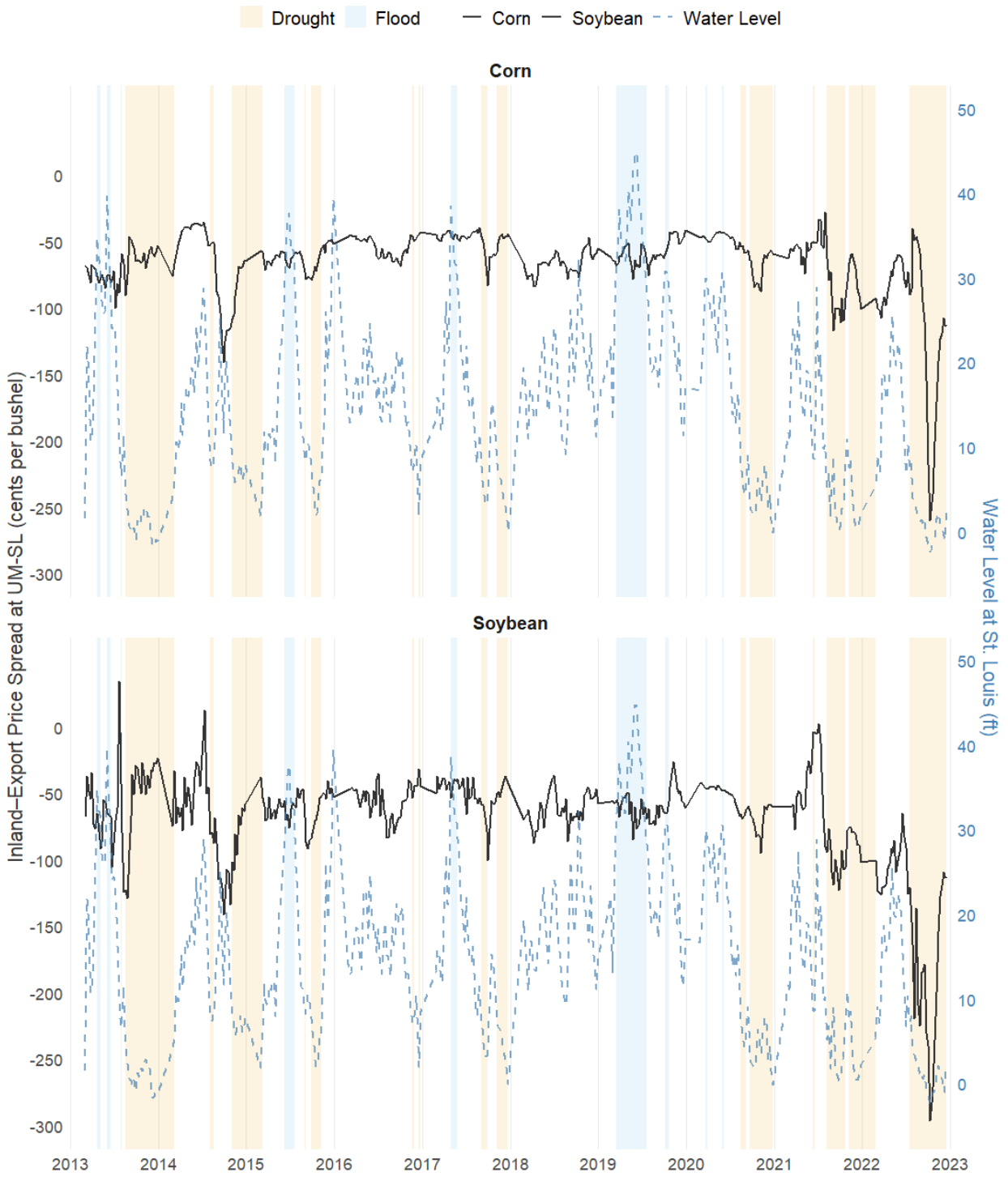
von Cramon-Taubadel, S., & Goodwin, B. K. (2021). Price transmission in agricultural markets. *Annual Review of Resource Economics*, *13*(1), 65–84. https://doi.org/10.1146/annurev-resource-100518-093938

Yu, T. (Edward), Bessler, D. A., & Fuller, S. W. (2007). Price Dynamics in U.S. Grain and Freight Markets. *Canadian Journal of Agricultural Economics/Revue Canadienne d'agroeconomie*, *55*(3), 381–397. https://doi.org/10.1111/j.1744-7976.2007.00098.x

Zellner, A. (1962). An Efficient Method of Estimating Seemingly Unrelated Regressions and Tests for Aggregation Bias. *Journal of the American Statistical Association*, *57*(298), 348–368. https://doi.org/10.2307/2281644

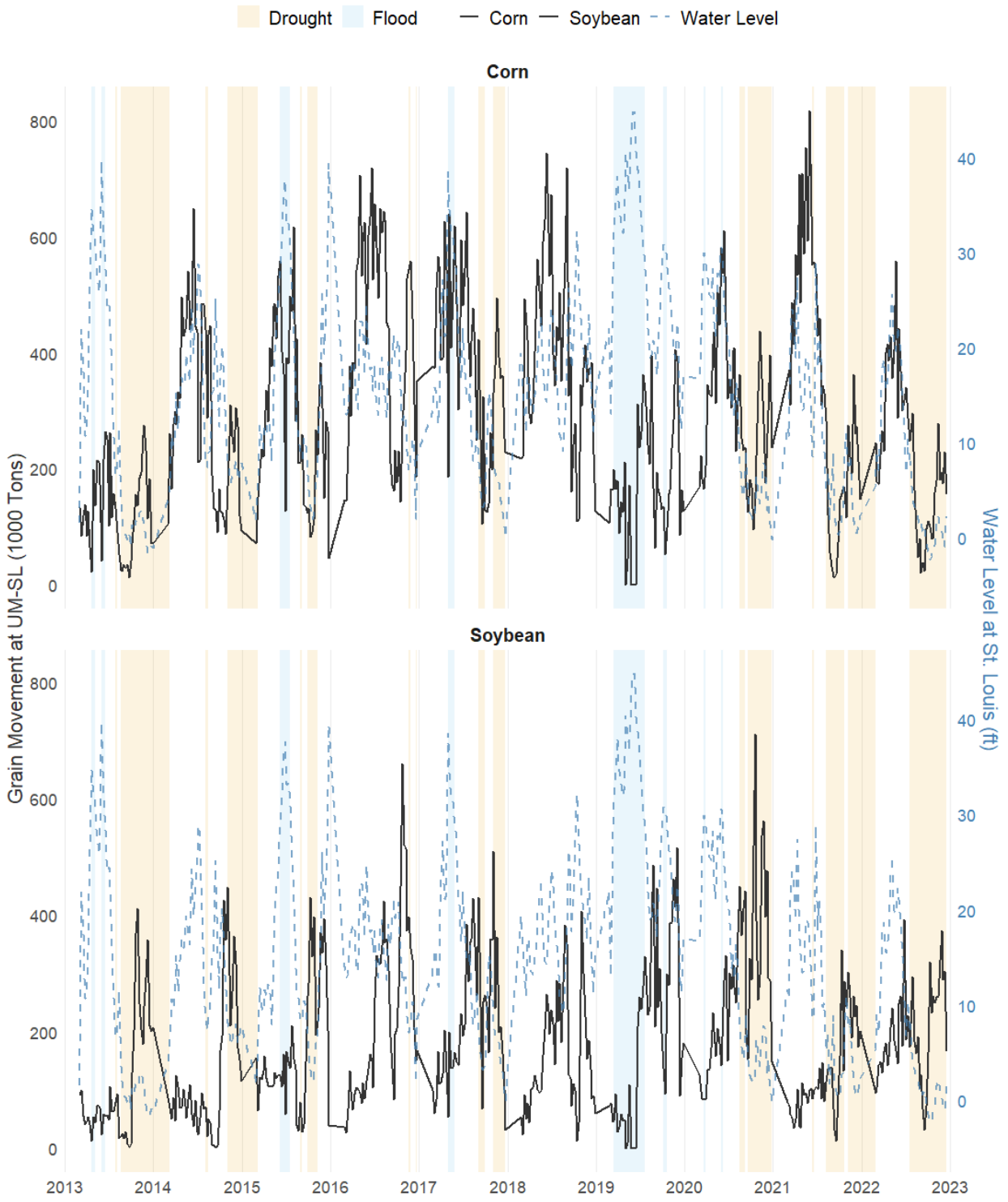
Figures

Figure 1. Weekly Water Level and Grain Elevator Price Spread at UM-SL, 2013-2022



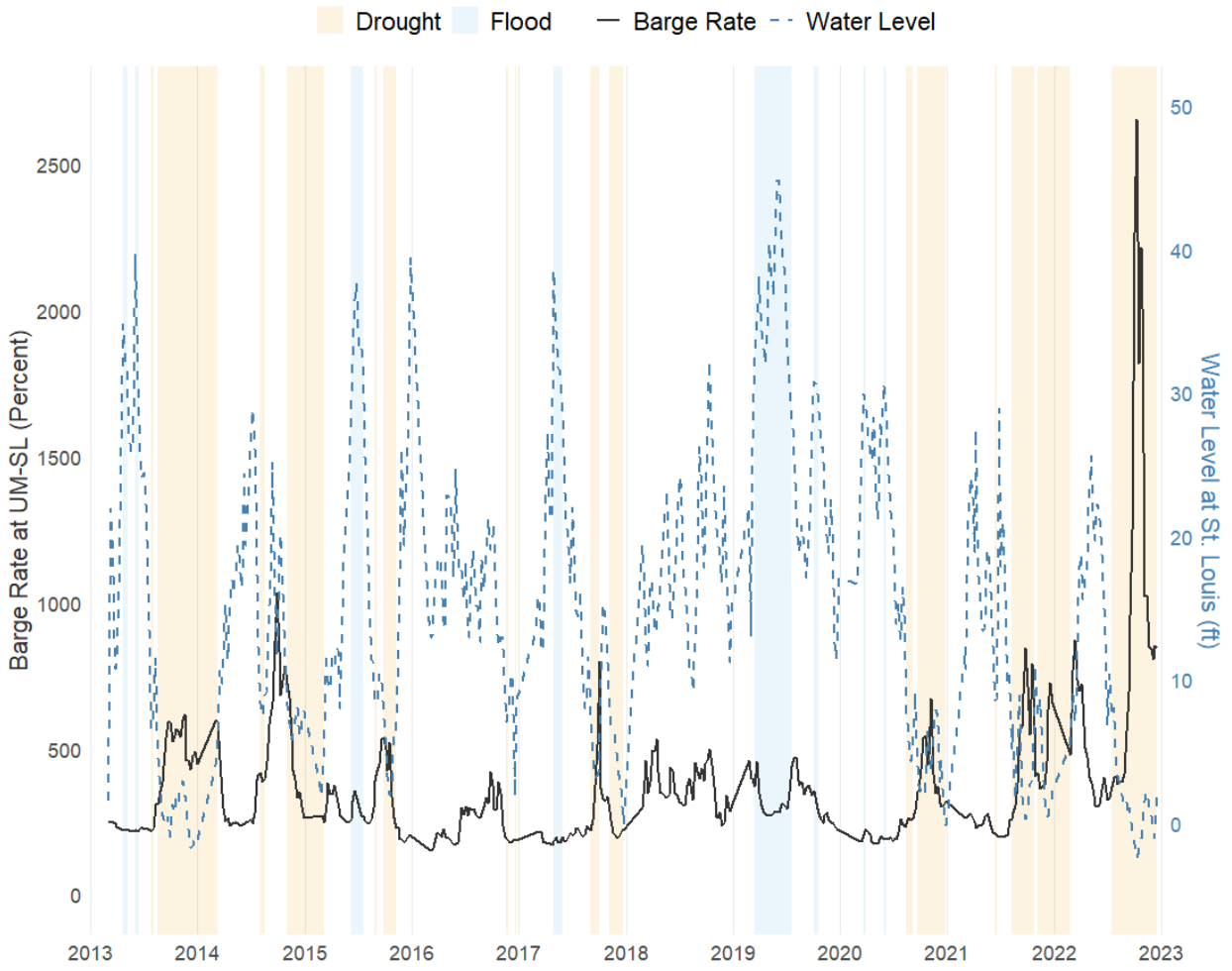
Note: The figures show temporal relationships between variables. Solid lines show UM-SL elevator inland-export spreads (cents/bu, left axis); dashed lines show St. Louis water levels (ft, right axis). January and February are excluded.

Figure 2. Weekly Water Level and Grain Downbound Movement at UM-SL, 2013-2022



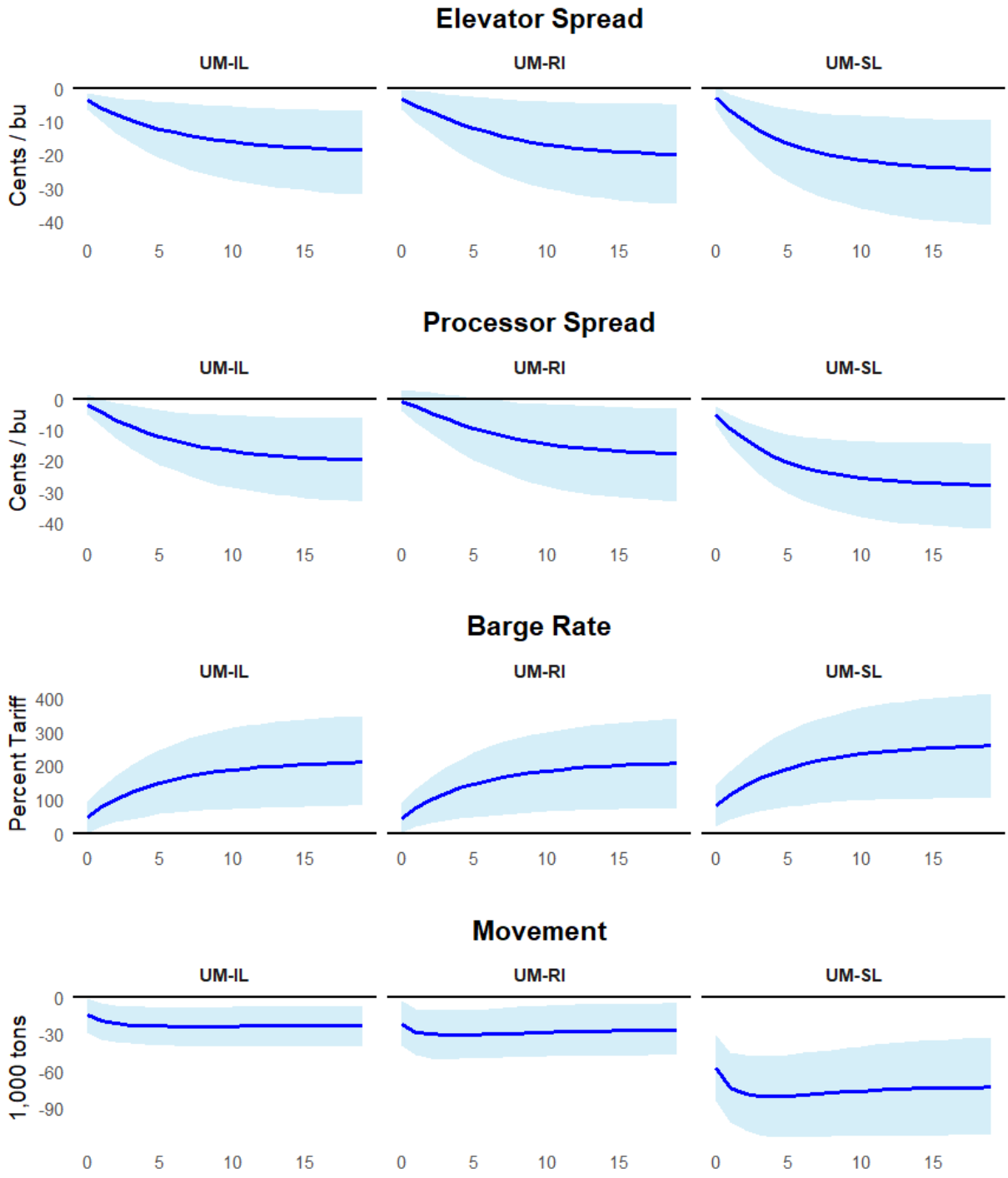
Note: The figures show temporal relationships between variables. Solid lines show UM-SL gain downbound barge movement (1000 tons, left axis); dashed lines show St. Louis water levels (ft, right axis). January and February are excluded.

Figure 3. Weekly Water Level and Grain Barge Rates at UM-SL, 2013-2022



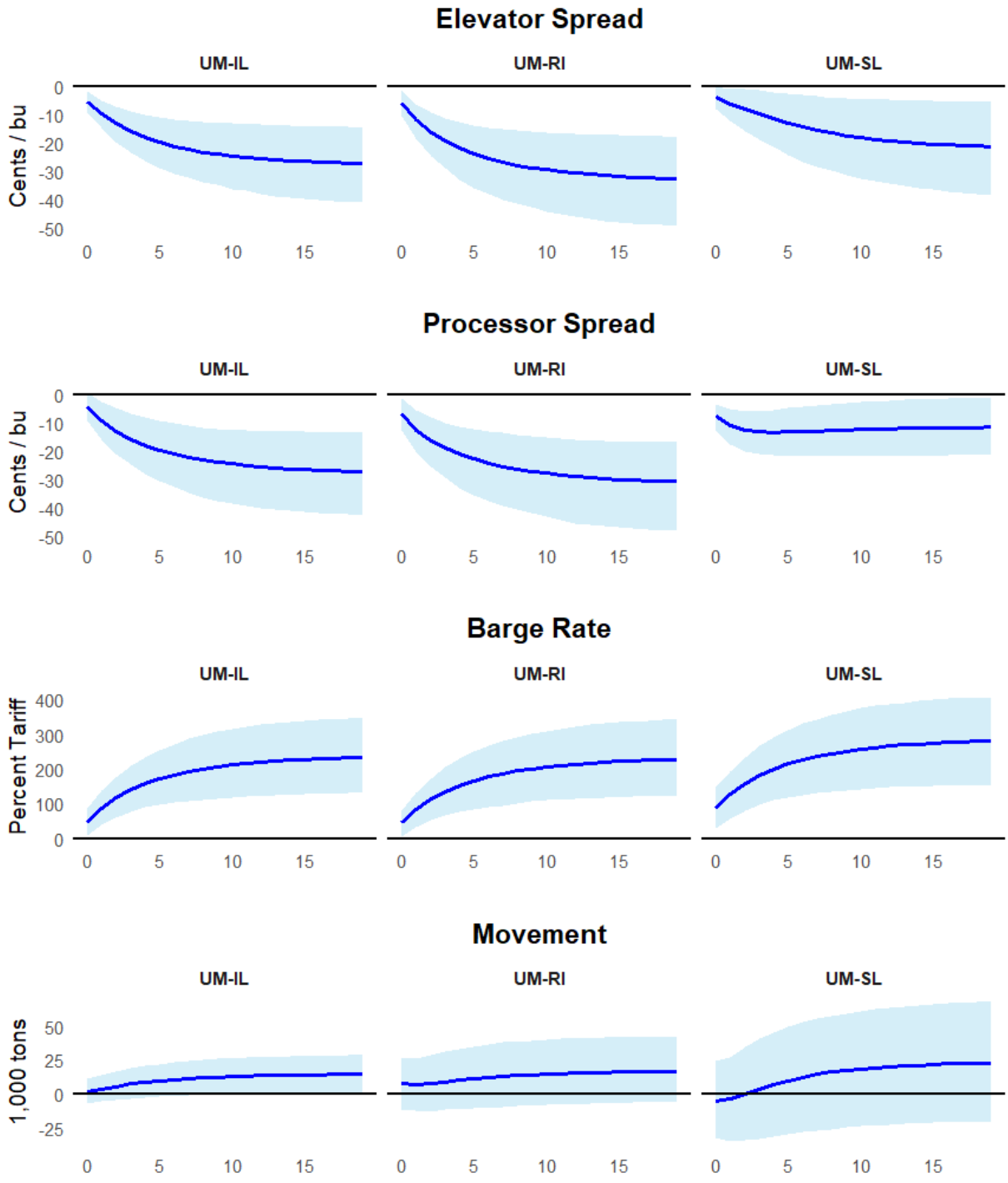
Note: The figures show temporal relationships between variables. Solid lines show UM-SL barge rates (percent, left axis); dashed lines show St. Louis water levels (ft, right axis). January and February are excluded.

Figure 4. Impulse Responses of Drought Shock: Corn



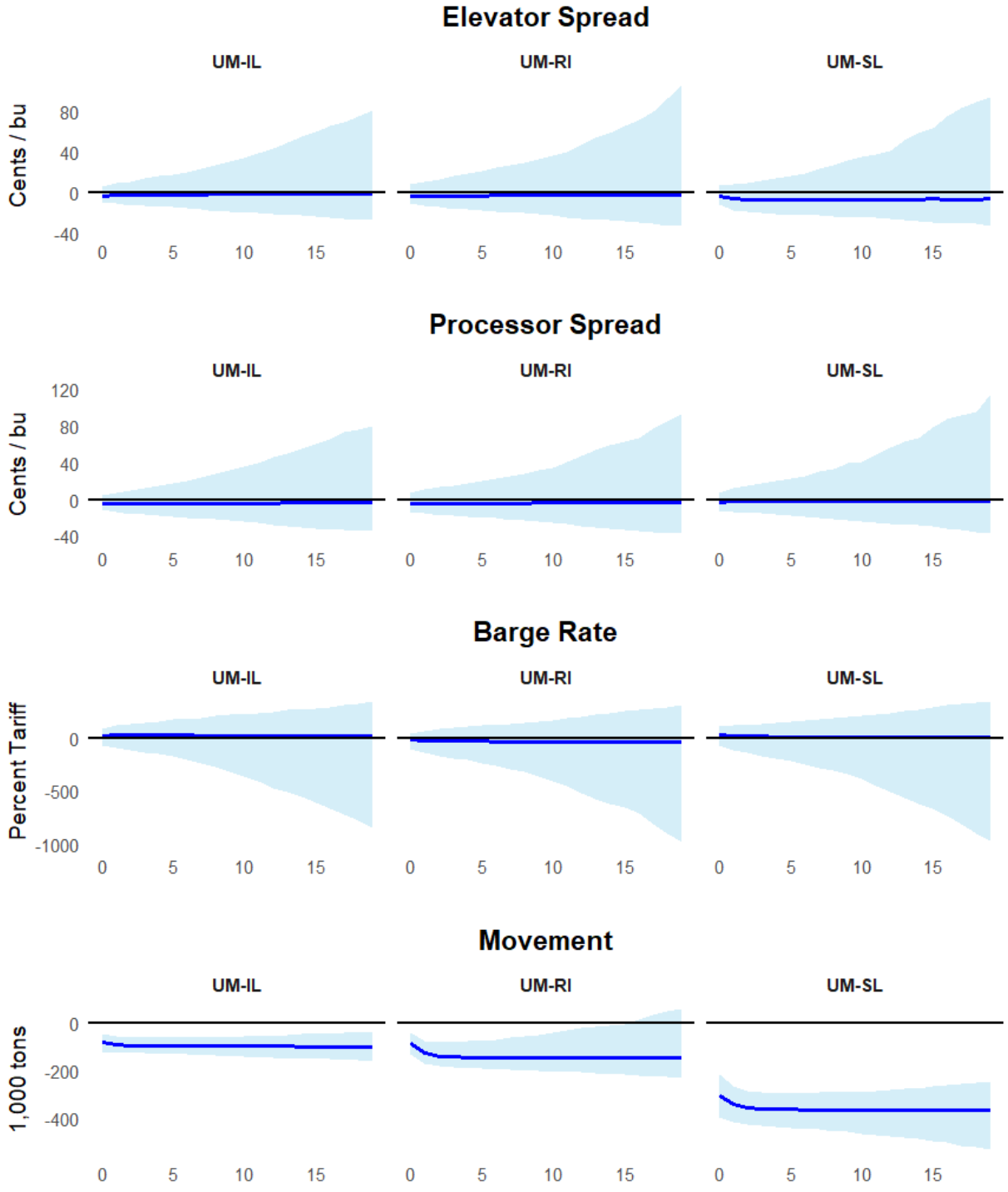
Note: The figures report the generalized impulse response functions (GIRFs) to a low-water shock, defined as a 15-foot decline in the St. Louis river stage from its sample median. Shaded areas indicate 95% confidence intervals based on stratified bootstrap procedures. All responses are expressed as deviations from their baseline paths.

Figure 5. Impulse Responses of Drought Shock: Soybean



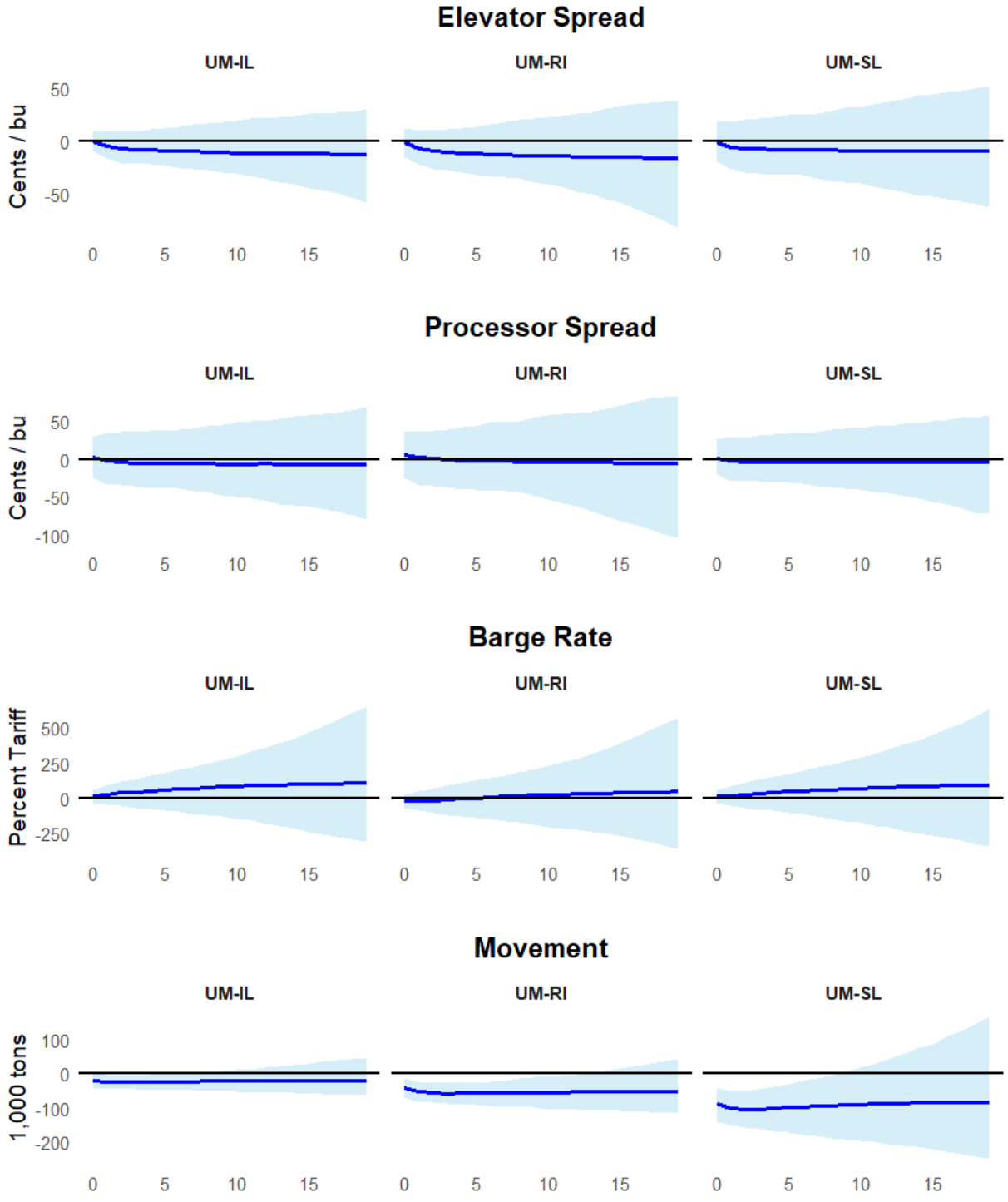
Note: The figures report the generalized impulse response functions (GIRFs) to a low-water shock, defined as a 15-foot decline in the St. Louis river stage from its sample median. Shaded areas indicate 95% confidence intervals based on stratified bootstrap procedures. All responses are expressed as deviations from their baseline paths.

Figure 6. Impulse Responses of Flood Shock: Corn



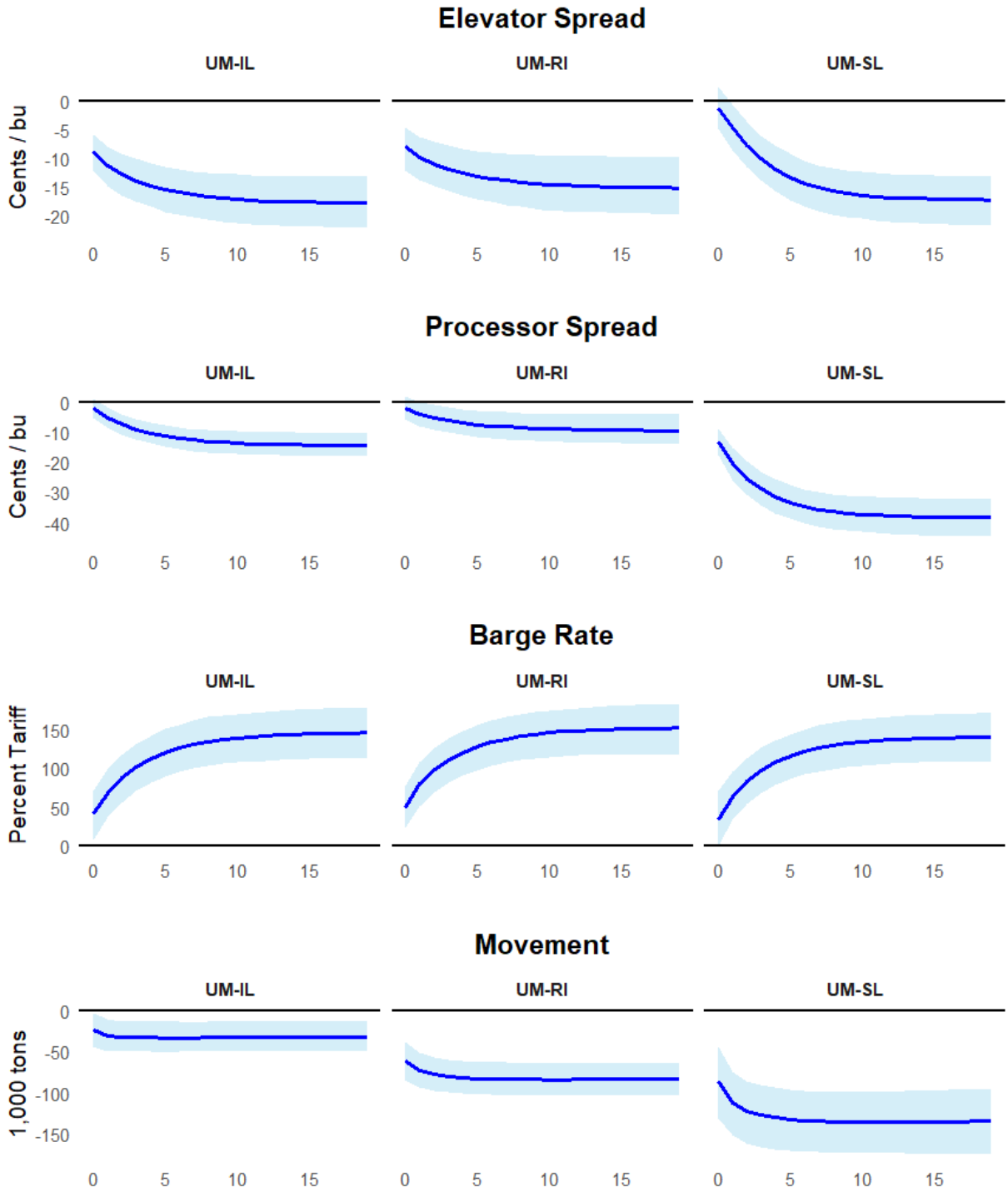
Note: The figures report the generalized impulse response functions (GIRFs) to a high-water shock, defined as an increase of river stage in the St. Louis river stage from its sample median to 40 feet. Shaded areas indicate 95% confidence intervals based on stratified bootstrap procedures. All responses are expressed as deviations from their baseline paths.

Figure 7. Impulse Responses of Flood Shock: Soybean



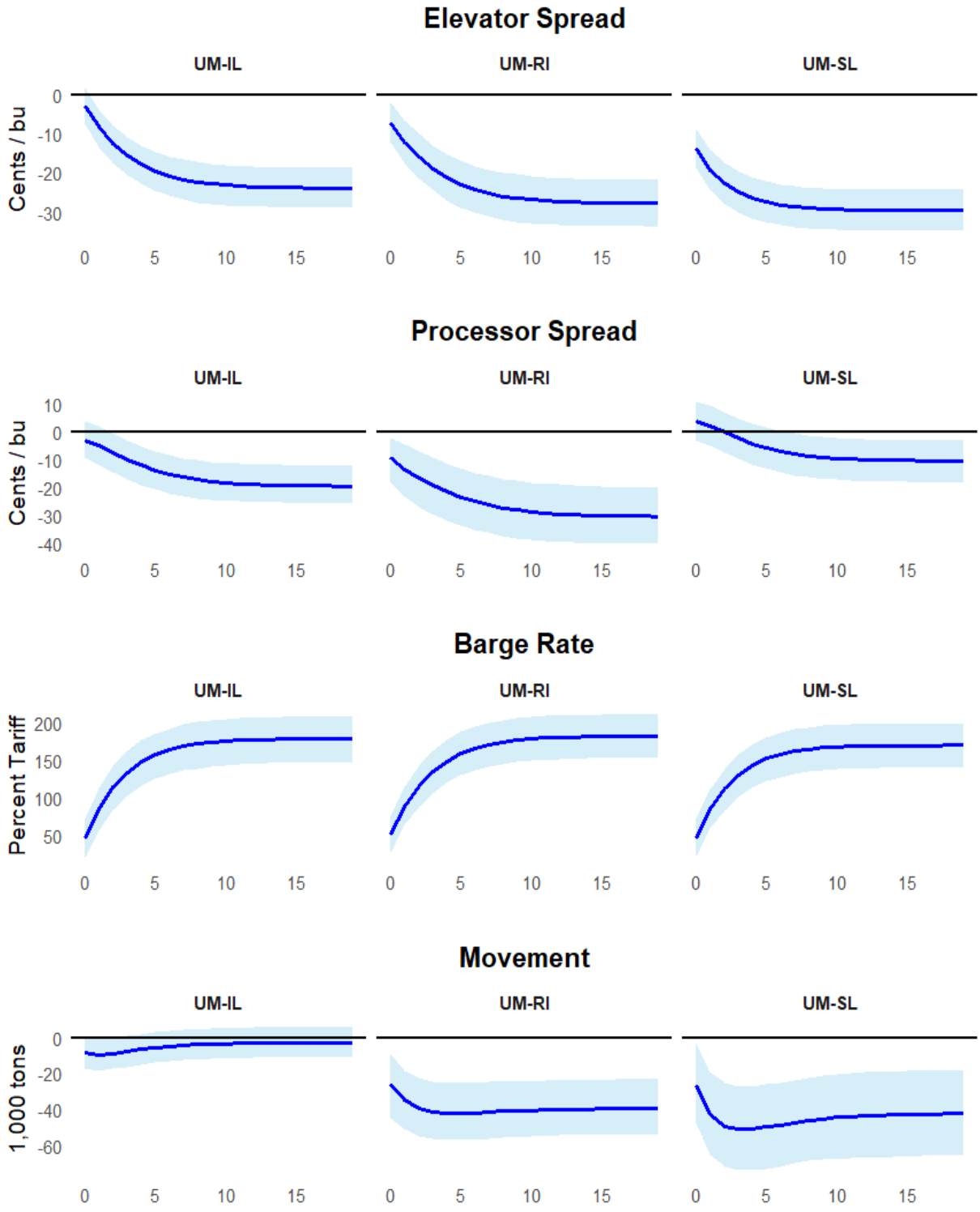
Note: The figures report the generalized impulse response functions (GIRFs) to a high-water shock, defined as an increase of river stage in the St. Louis river stage from its sample median to 40 feet. Shaded areas indicate 95% confidence intervals based on stratified bootstrap procedures. All responses are expressed as deviations from their baseline paths.

Figure 8. Impulse Responses of Energy Shock: Corn



Note: The figures report the generalized impulse response functions (GIRFs) to an energy shock, defined as the Midwest diesel price from its sample median to $5 per gallon. Shaded areas indicate 95% confidence intervals based on stratified bootstrap procedures. All responses are expressed as deviations from their baseline paths

Figure 9. Impulse Responses of Energy Shock: Soybean



Note: The figures report the generalized impulse response functions (GIRFs) to an energy shock, defined as the Midwest diesel price from its sample median to $5 per gallon. Shaded areas indicate 95% confidence intervals based on stratified bootstrap procedures. All responses are expressed as deviations from their baseline paths

Tables

Table 1 Summary Statistics

	Mean	Median	Min	Max	St.Dev.	N
			Panel A - Global Variables			
Water Level (ft)	15.19	15.02	-2.35	44.82	10.12	442
Diesel Price ($/gallon)	3.21	3.01	1.94	5.78	0.84	442
			Panel B - Corn			
UM-RI						
E. Spread (Cents/bu)	-78.55	-74.39	-230.21	8.98	26.05	442
P. Spread (Cents/bu)	-63.23	-60.20	-218.14	35.50	26.39	442
B. Rate (Percent)	462.60	406.75	235.00	2033.33	225.30	442
B. Move (1,000 tons)	105.23	74.25	0.00	398.20	101.40	442
UM-SL						
E. Spread (Cents/bu)	-65.47	-60.18	-259.33	-27.41	26.66	442
P. Spread (Cents/bu)	-78.60	-73.88	-234.80	-31.55	29.69	442
B. Rate (Percent)	370.42	300.00	152.50	2653.12	260.94	442
B. Move (1,000 tons)	298.91	275.96	0.00	817.70	173.89	442
UM-IL						
E. Spread (Cents/bu)	-75.86	-72.06	-227.65	-5.41	25.20	442
P. Spread (Cents/bu)	-65.72	-62.45	-221.35	-2.36	24.36	442
B. Rate (Percent)	452.47	395.50	225.00	2075.00	233.71	442
B. Move (1,000 tons)	95.26	86.45	0.00	361.20	68.70	442
			Panel C - Soybean			
UM-RI						
E. Spread (Cents/bu)	-99.76	-93.01	-291.19	24.28	34.95	442
P. Spread (Cents/bu)	-84.29	-77.10	-275.90	209.50	47.53	442
B. Rate (Percent)	462.60	406.75	235.00	2033.33	225.30	442
B. Move (1,000 tons)	78.05	56.80	0.00	454.70	78.76	442
UM-SL						
E. Spread (Cents/bu)	-68.40	-59.93	-295.71	34.64	38.00	442
P. Spread (Cents/bu)	-48.81	-49.00	-154.50	113.75	29.03	442
B. Rate (Percent)	370.42	300.00	152.50	2653.12	260.94	442
B. Move (1,000 tons)	180.47	150.40	0.00	710.60	126.85	442
UM-IL						
E. Spread (Cents/bu)	-89.59	-83.63	-257.14	4.96	30.88	442
P. Spread (Cents/bu)	-70.55	-64.60	-256.60	109.44	37.33	442
B. Rate (Percent)	452.47	395.50	225.00	2075.00	233.71	442
B. Move (1,000 tons)	45.04	34.90	0.00	219.90	40.56	442

Note: This table reports summary statistics for weekly raw data from 2013 to 2022. Panel A presents global variables, including St. Louis river stage and Midwest diesel prices. Panels B and C report regional corn and soybean variables for the UM-RI, UM-SL, and UM-IL regions. E. Spread and P. Spread denote elevator and processor price spreads, respectively; B. Rate denotes barge rates; and B. Move denotes barge movements. Price spreads are inland cash prices minus Gulf export prices, measured in cents per bushel. Barge rates are tariff-index percentages, and barge movements are measured in thousand tons.

Table 2. Hydrological regime composition

	Definition	# of weeks
Drought	Water level<=9ft	135
Normal	9ft < Water level <=28ft	258
Flood	Water level > 28ft	49
Total	--	442

Note: This table reports the number of weekly observations classified as drought, normal, or flood based on fixed river-stage thresholds at the St. Louis gauge. The thresholds reflect navigation and flood-stage benchmarks; see the Method and Empirical Approach section for details. These classifications are used to estimate regime-dependent dynamics in the MR-GVAR framework.

Appendix A

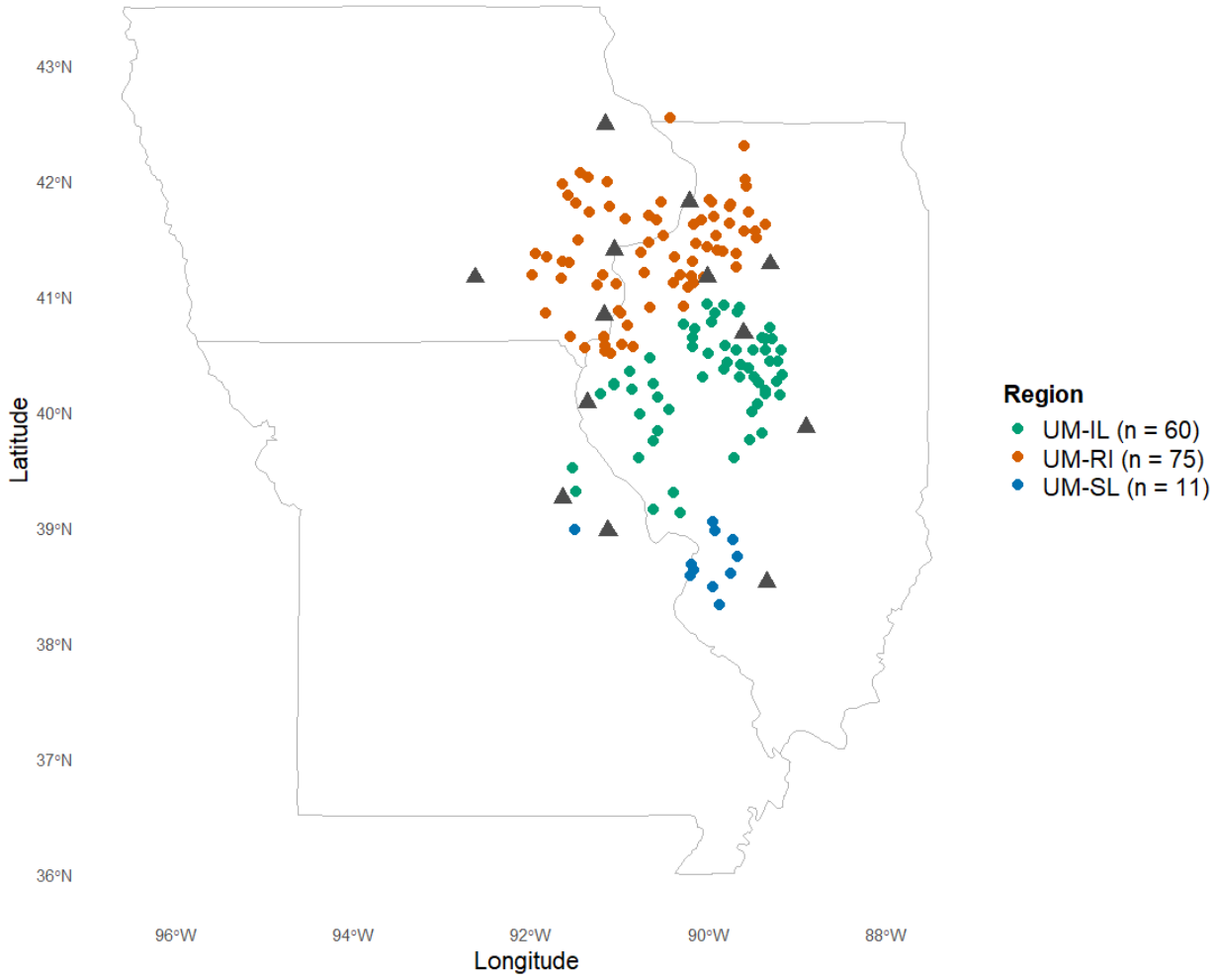
Figure A1. Upper Mississippi River Locks system.



Note: This figure shows the locks and dams of the Mississippi River and the Illinois River from the Upper Mississippi River system, retrieved from: https://upload.wikimedia.org/wikipedia/commons/0/09/Upper_Mississippi_Lock_and_dams.jpeg

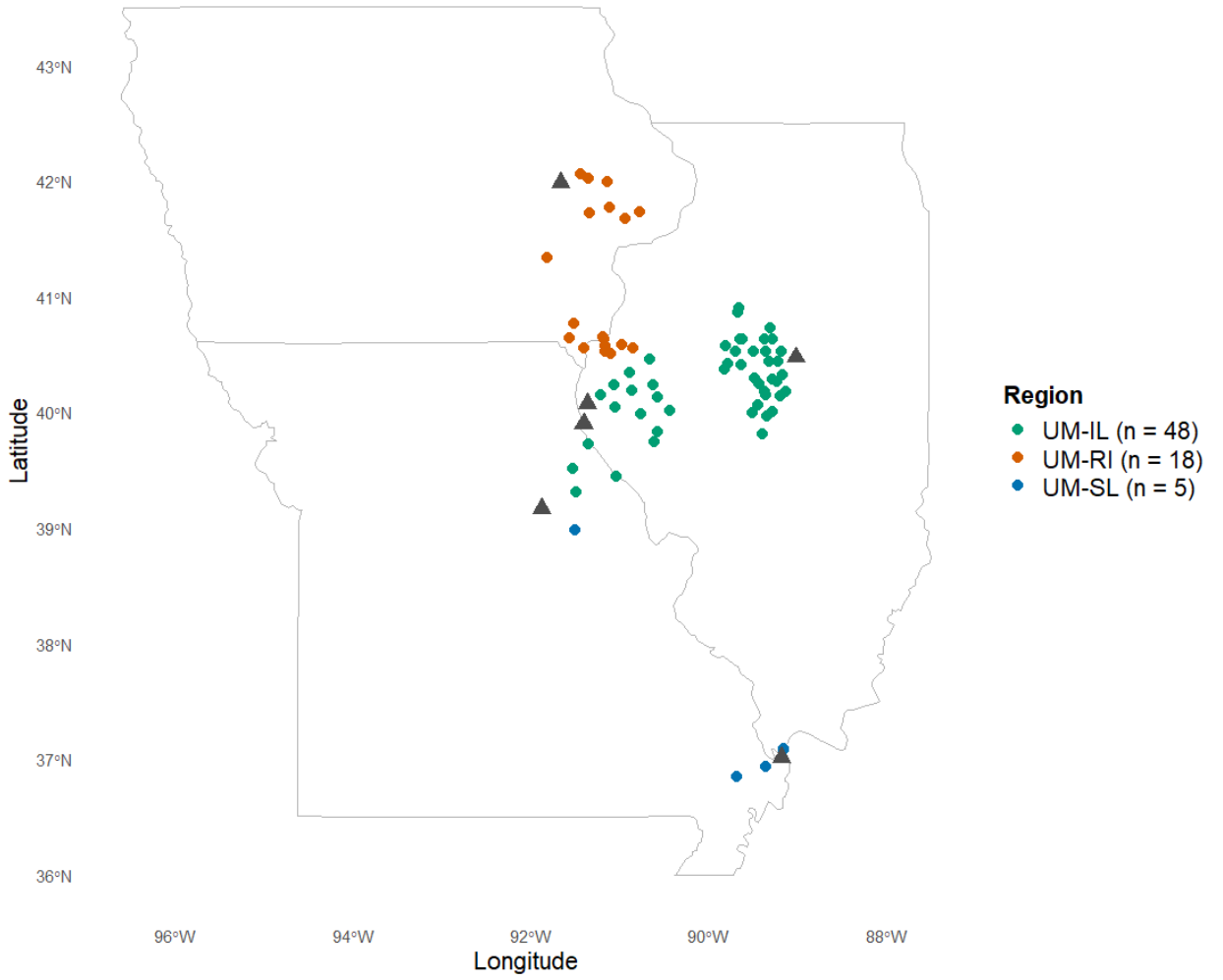
Appendix B. Figures

Figure B1. Corn Elevators and Processors Map



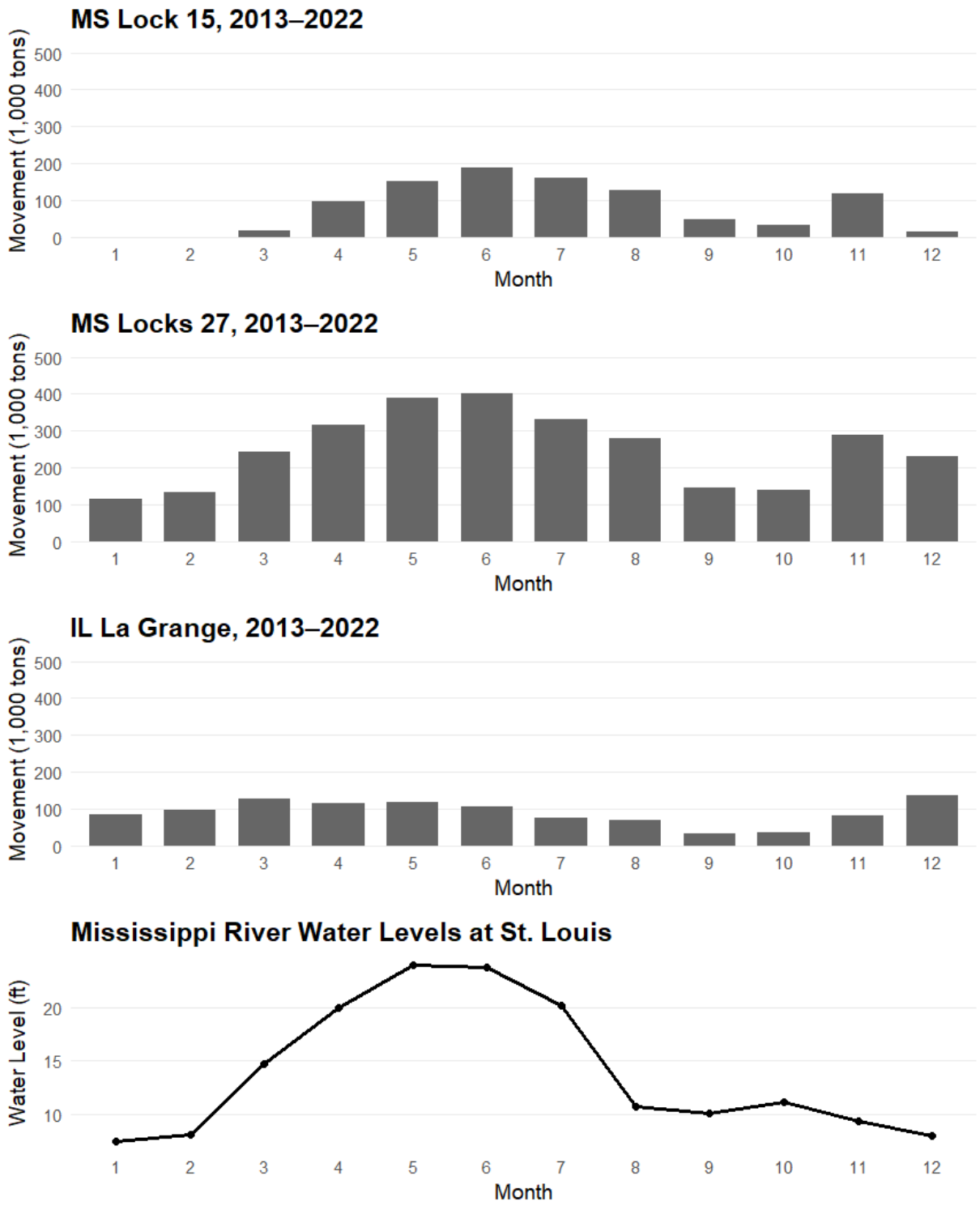
Note: This figure displays the distribution and number of corn elevators by region, using a 50-mile identification distance, marked as dots. Triangles represent corn processors. The processors could be included in two different regions.

Figure B2. Soybean Elevators and Processors Map



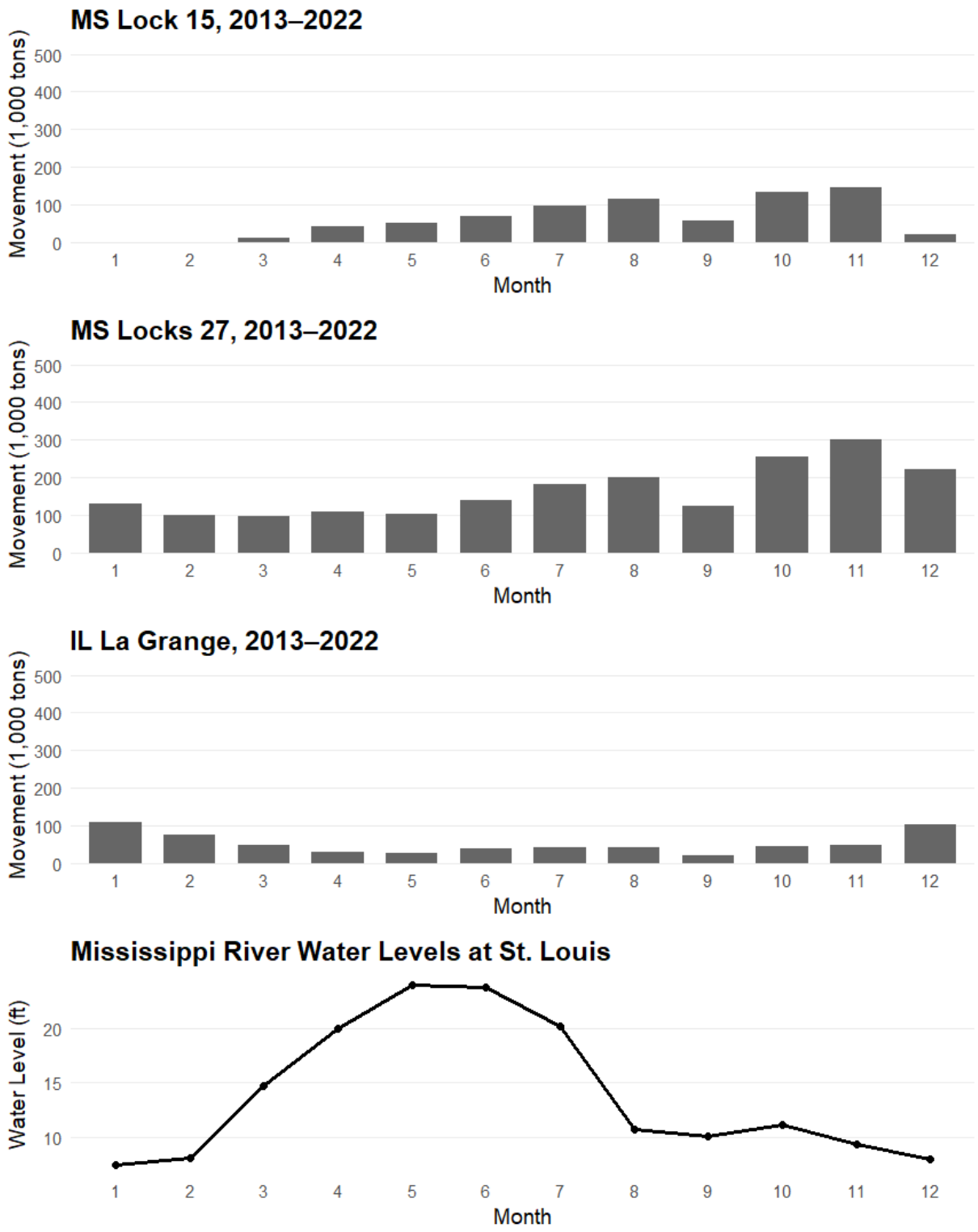
Note: This figure displays the distribution and number of soybean elevators by region, using a 50-mile identification distance, marked as dots. Triangles represent soybean processors. The processors may be assigned to two regions.

Figure B3. Monthly Average Downbound Corn Barge Movements



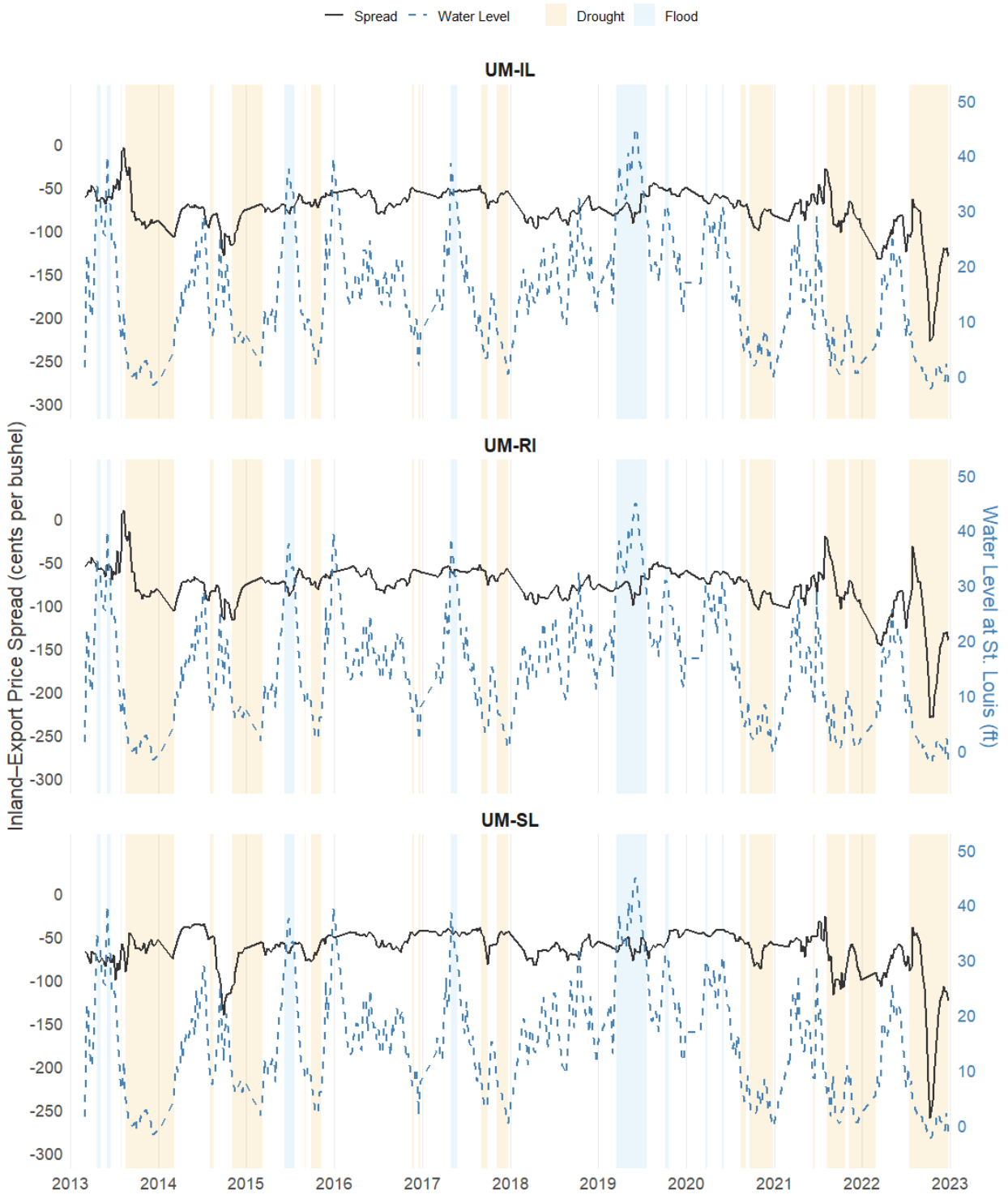
Note: The figures display the monthly average corn tonnage (1,000 metric tons) moved through Lock 15, Lock 27, and Lock La Grange, as well as the monthly average water level (ft) in St. Louis. Data covers from 2013 to 2022.

Figure B4. Monthly Average Downbound Soybean Barge Movements



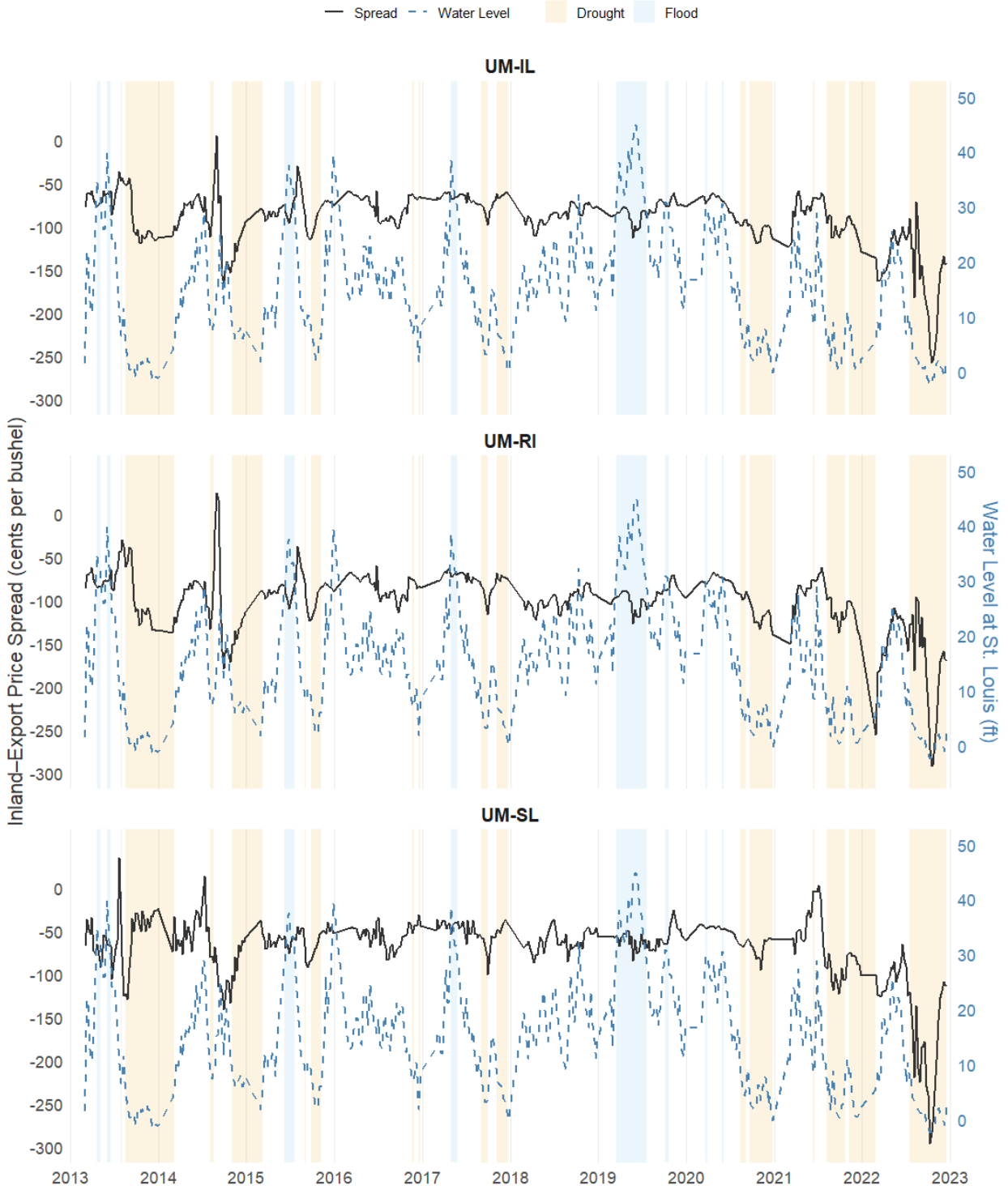
Note: The figures display the monthly average soybean tonnage (1,000 metric tons) moved through Lock 15, Lock 27, and Lock La Grange, as well as the monthly average water level (ft) in St. Louis. Data covers from 2013 to 2022.

Figure B5 Weekly Water Level and Corn Elevator Price Spreads, 2013-2022



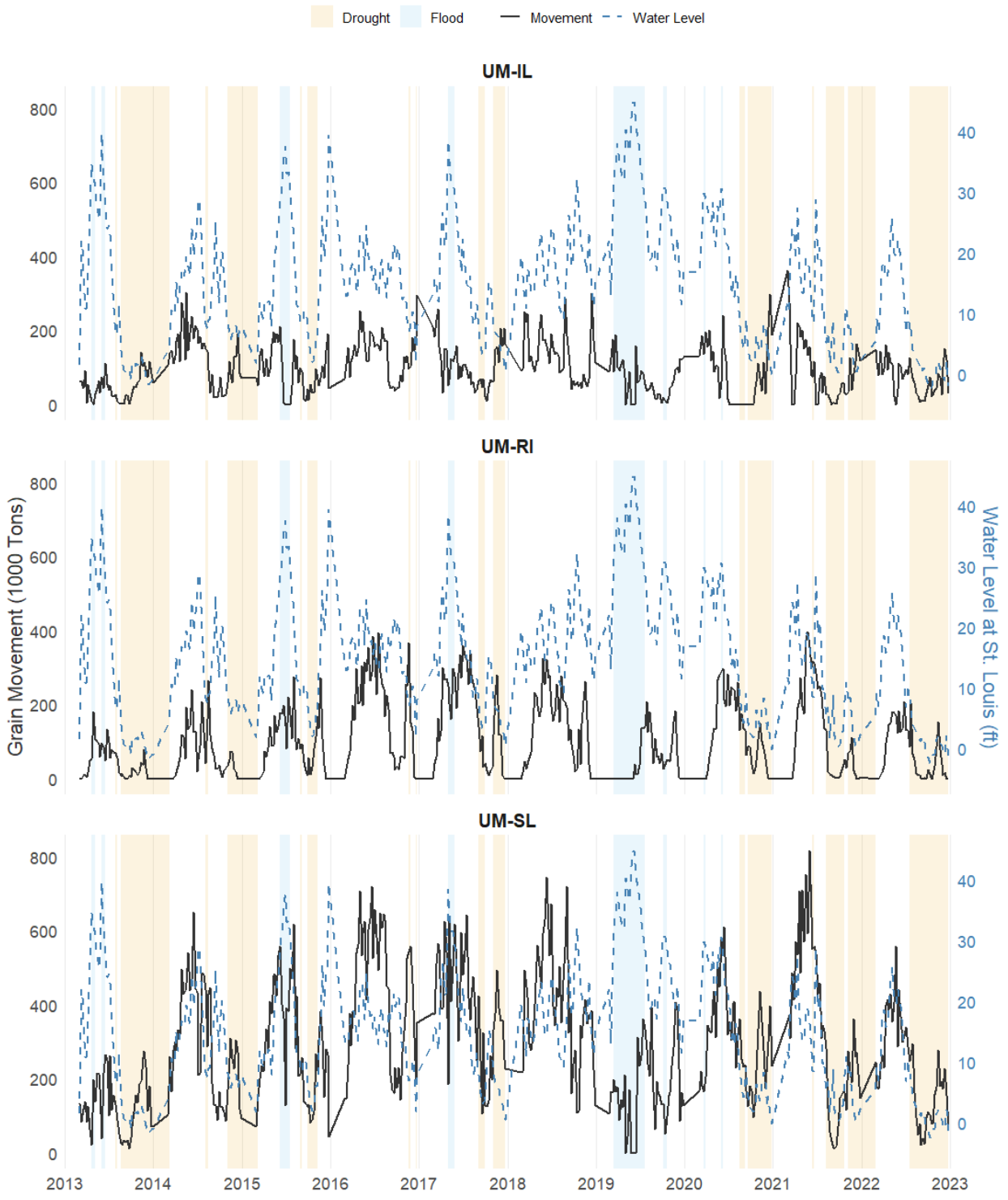
Note: The figures show temporal relationships between variables. Solid lines show corn elevator inland-export price spread (cents/bu, left axis); dashed lines show St. Louis water levels (ft, right axis). January and February are excluded.

Figure B6 Weekly Water Level and Soybean Elevator Price Spreads, 2013-2022



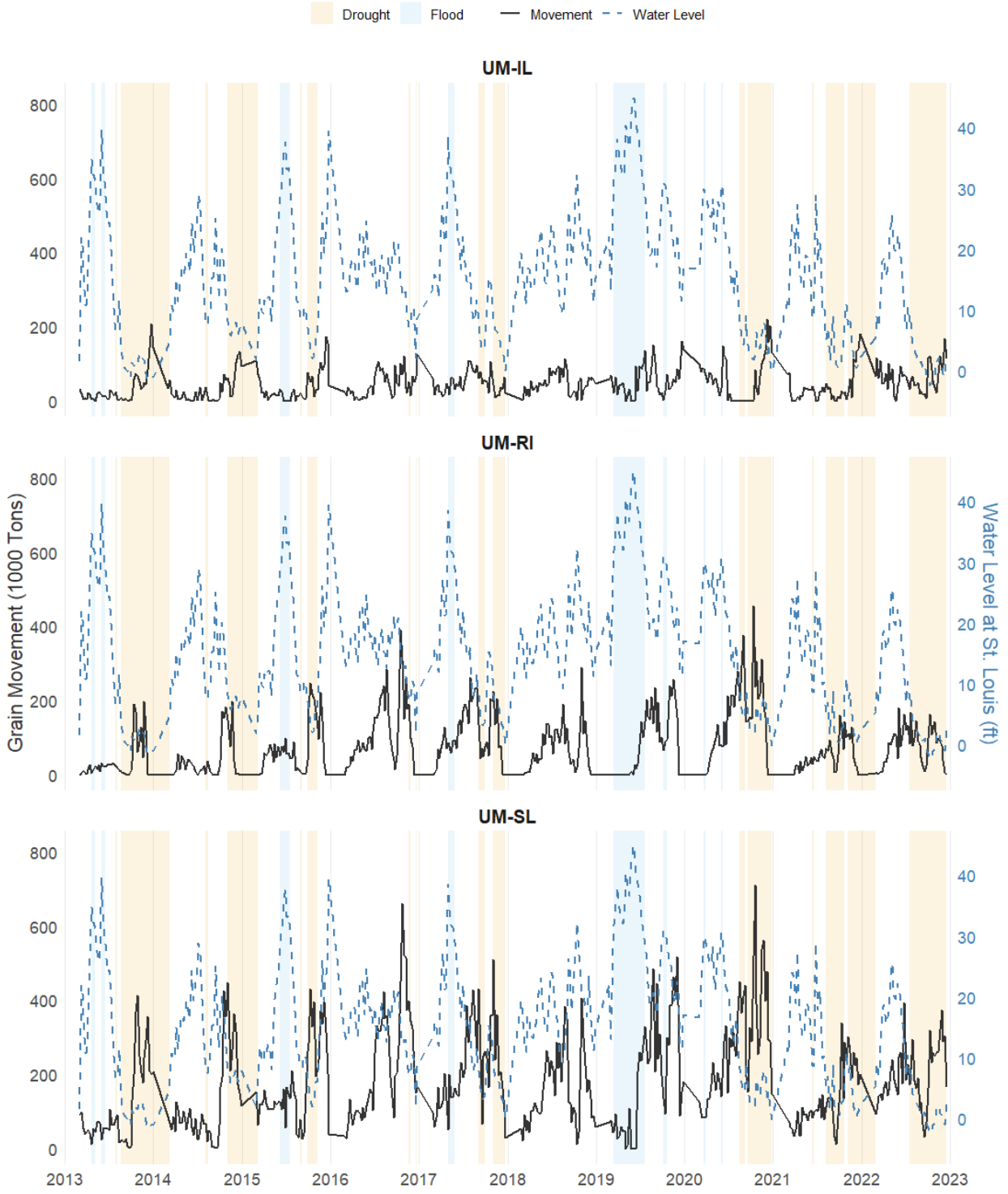
Note: The figures show temporal relationships between variables. Solid lines show soybean elevator inland-export price spread (cents/bu, left axis); dashed lines show St. Louis water levels (ft, right axis). January and February are excluded.

Figure B7 Weekly Water Level and Corn Movements, 2013-2022



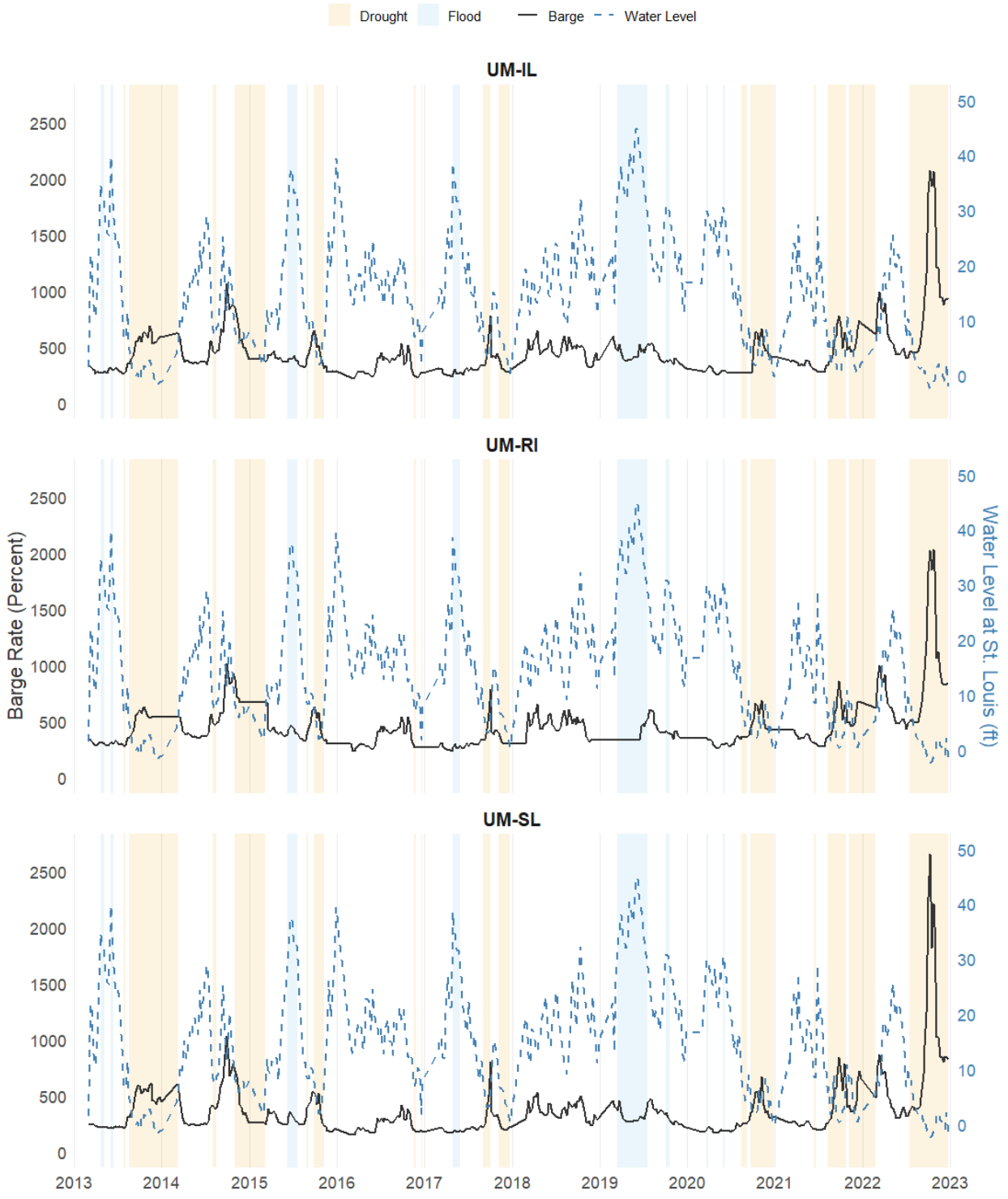
Note: The figures show temporal relationships between variables. Solid lines show corn downbound barge movements (1000 tons, left axis); dashed lines show St. Louis water levels (ft, right axis). January and February are excluded.

Figure B8 Weekly Water Level and Soybean Movements, 2013-2022



Note: Solid lines show soybean downbound barge movements (1000 tons, left axis); dashed lines show St. Louis water levels (ft, right axis). January and February are excluded.

Figure B9 Weekly Water Level and Downbound Grain Barge Rate, 2013-2022



Note: Solid lines show downbound grain barge rates (percent, left axis); dashed lines show St. Louis water levels (ft, right axis). January and February are excluded.

Appendix C. Conditional MR-GVAR

Dees et al. (2007) describe a framework for constructing a conditional global vector autoregressive (GVAR) model in which each region-specific model is specified conditional on the set of cross-sectional region-specific foreign variables. Following this framework, we construct a conditional MR-GVAR. We begin by considering the joint estimation of y_{it}^{ds} and $y^{ds^*}_{it}$ in the following system:

$$\begin{cases} y_{i,t}^{ds} = a_i + \Phi_i\, y_{i,t-1}^{ds} + \Lambda_i\, y_{i,t}^{ds*} + \Gamma_i y_{i,t-1}^{ds*} + \beta_i\, x_{i,t} + \varepsilon_{i,t} \\ y_{i,t}^{ds*} = a_i^* + \Phi_i^* y_{i,t-1}^{ds} + \Gamma_i^* y_{i,t-1}^{ds*} + \beta_i{}^* x_{i,t} + \varepsilon_{i,t}^* \end{cases}, \tag{C1}$$

in which $\begin{bmatrix} \varepsilon_{i,t} \\ \varepsilon_{i,t}^* \end{bmatrix} \sim iid(0, \Sigma_{ii})$, and $\Sigma_{ii} = \begin{bmatrix} \Sigma_{ii}^{yy} & \Sigma_{ii}^{yy^*} \\ \Sigma_{ii}^{y^*y} & \Sigma_{ii}^{y^*y^*} \end{bmatrix}$ is the joint covariance matrix. The conditional model for $y_{i,t}^{ds} | y^{ds^*}_{i,t}$ is then specified as:

$$E\left[y_{i,t}^{ds} | y^{ds^*}_{i,t}, Information\ set_{t-1} \right]$$

$$= a_i + \Phi_i\, y_{i,t-1} + \Lambda_i\, y_{i,t}^{ds*} + \Gamma_i\, y_{i,t-1}^{ds*} + \beta_i\, x_{i,t} + E\left[\varepsilon_{i,t} | y^{ds^*}_{i,t},\ Information\ set_{t-1} \right]. \tag{C2}$$

Based on the joint covariance matrix we obtain:

$$E\left[\varepsilon_{i,t} | y^{ds^*}_{i,t},\ Information\ set_{t-1} \right] = \Sigma_{ii}^{yy^*} \Sigma_{ii}^{y^*y^{*-1}} \varepsilon_{i,t}^*$$

$$= \Sigma_{ii}^{yy^*} \Sigma_{ii}^{y^*y^{*-1}} (y^{ds^*}_{i,t} - a_i^* - \Phi_i^* y_{i,t-1} - \Gamma_i y_{i,t-1}^{ds*} - \beta_i{}^* x_{i,t}). \tag{C3}$$

Substituting (C3) into (C2) yields:

$$E\left[y_{i,t}^{ds} | y_{i,t}^{ds*} \right] = a_i + \Phi_i\, y_{i,t-1} + \Lambda_i\, y_{i,t}^{ds*} + \Gamma_i\, y_{i,t-1}^{ds*} + \beta_i\, x_{i,t} + \Sigma_{ii}^{yy^*} \Sigma_{ii}^{y^*y^{*-1}} (y_{i,t}^{ds*} - a_i^* -$$

$$\Phi_i^* y_{i,t-1} - \Gamma_i y_{i,t-1}^{ds*} - \beta_i{}^* x_{i,t}). \tag{C4}$$

By defining:

$$v_{i,t} = y_{i,t}^{ds} - E\left[y_{i,t}^{ds} | y_{i,t}^{ds*}, Information\ set_{t-1}\right], \quad \text{(C5)}$$

and constructing:

$$E\left[v_{i,t} | y^{ds*}_{i,t}, y_{i,t-1}^{ds}, y_{i,t-1}^{ds*}\right] = 0, \quad \text{(C6)}$$

we finally get:

$$y_{i,t}^{ds} = a_i + \Phi_i\, y_{i,t-1} + \Lambda_i\, y_{i,t}^{ds*} + \Gamma_i\, y_{i,t-1}^{ds*} + \beta_i\, x_{i,t} + \Sigma_{ii}^{yy^*} \Sigma_{ii}^{y^*y^{*-1}} \left(y^{ds*}_{i,t} - a_i^* - \Phi_i^* y_{i,t-1} - \Gamma_i^* y_{i,t-1}^{ds*} - \beta_i{}^* x_{i,t}\right) + v_{i,t}. \quad \text{(C7)}$$

Rearranging the terms, the model can be written as:

$$y_{i,t}^{ds} = \lambda_i + \Upsilon_i^1\, y_{i,t-1} + \Upsilon_i^2 y_{i,t}^{ds*} + \Upsilon_i^3\, y_{i,t-1}^{ds*} + \Upsilon_i^4 x_{i,t} + v_{i,t}, \quad \text{(C8)}$$

in which $\lambda_i = a_i - \Sigma_{ii}^{yy^*} \Sigma_{ii}^{y^*y^{*-1}} a_i^*$, $\Upsilon_i^1 = \Phi_i - \Sigma_{ii}^{yy^*} \Sigma_{ii}^{y^*y^{*-1}} \Phi_i^*$, $\Upsilon_i^2 = \Lambda_i + \Sigma_{ii}^{yy^*} \Sigma_{ii}^{y^*y^{*-1}}$, $\Upsilon_i^3 = \Gamma_i - \Sigma_{ii}^{yy^*} \Sigma_{ii}^{y^*y^{*-1}} \Gamma_i^*$, $\Upsilon_i^4 = \beta_i - \Sigma_{ii}^{yy^*} \Sigma_{ii}^{y^*y^{*-1}} \beta_i{}^*$. The constructed estimators λ_i, Υ_i^1, Υ_i^2, Υ_i^3, Υ_i^4 are then used for the impulse response analysis. $v_{i,t}$ is calculated for bootstrapping. To extend the conditional framework to the MR-GVAR setting, regime dependence is introduced by allowing the parameters in (C1) to vary with the regime indicator $r(t)$.

Appendix D. Cointegration Tests

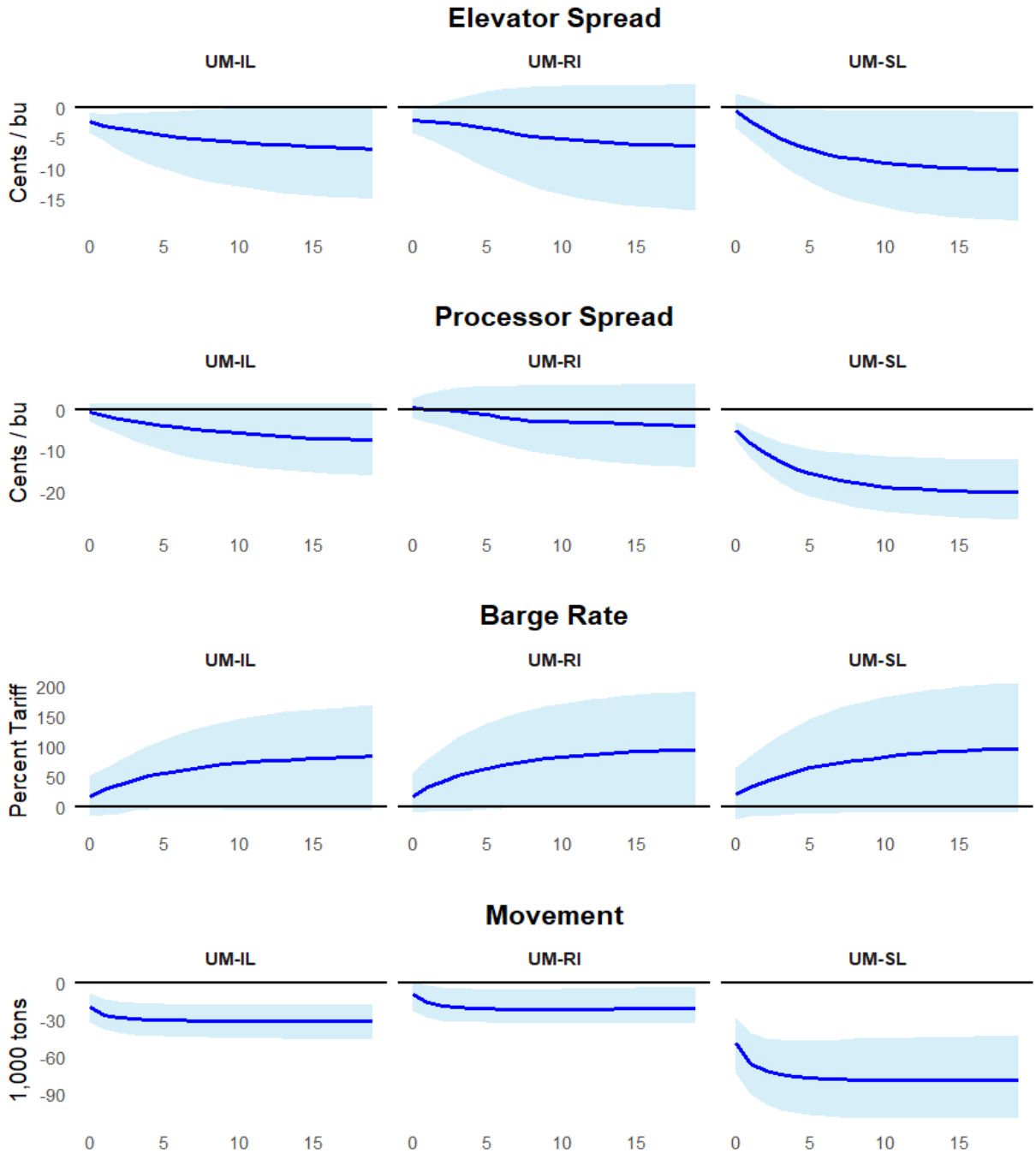
Table D1. Johansen Cointegration tests

H0	H1	Mid	Lower	Illinois
		Corn		
Eigenvalue				
r=0	r=1	75.34***	67.00***	91.93***
r<1	r=2	75.04***	42.70***	61.05***
r<=2	r=3	36.64***	39.93***	58.75***
r<=3	r=4	12.14**	18.79***	14.30**
Trace				
r=0	r=1	119.17***	168.42***	226.03***
r<1	r=2	123.83***	101.42***	134.10***
r<=2	r=3	48.79***	58.72***	73.05***
r<=3	r=4	12.14**	18.79***	14.30**
		Soybean		
Eigenvalue				
r=0	r=1	96.91***	84.92***	73.48***
r<1	r=2	45.93***	54.88***	58.66***
r<=2	r=3	27.41***	52.99***	46.29***
r<=3	r=4	18.66***	11.39***	15.94***
Trace				
r=0	r=1	118.90***	204.18***	194.37***
r<1	r=2	91.99**	119.27***	120.89***
r<=2	r=3	46.06***	64.39***	62.23***
r<=3	r=4	18.66***	11.39***	15.94***

Note: This table reports Johansen (1988, 1991) cointegration trace test results for a system of elevator and processor inland–export spreads, barge freight rates, and barge shipment volumes. Tests are based on a VAR(2) specification with an unrestricted intercept and no deterministic trend. The null hypothesis of at most (r) cointegrating relationships is evaluated sequentially.

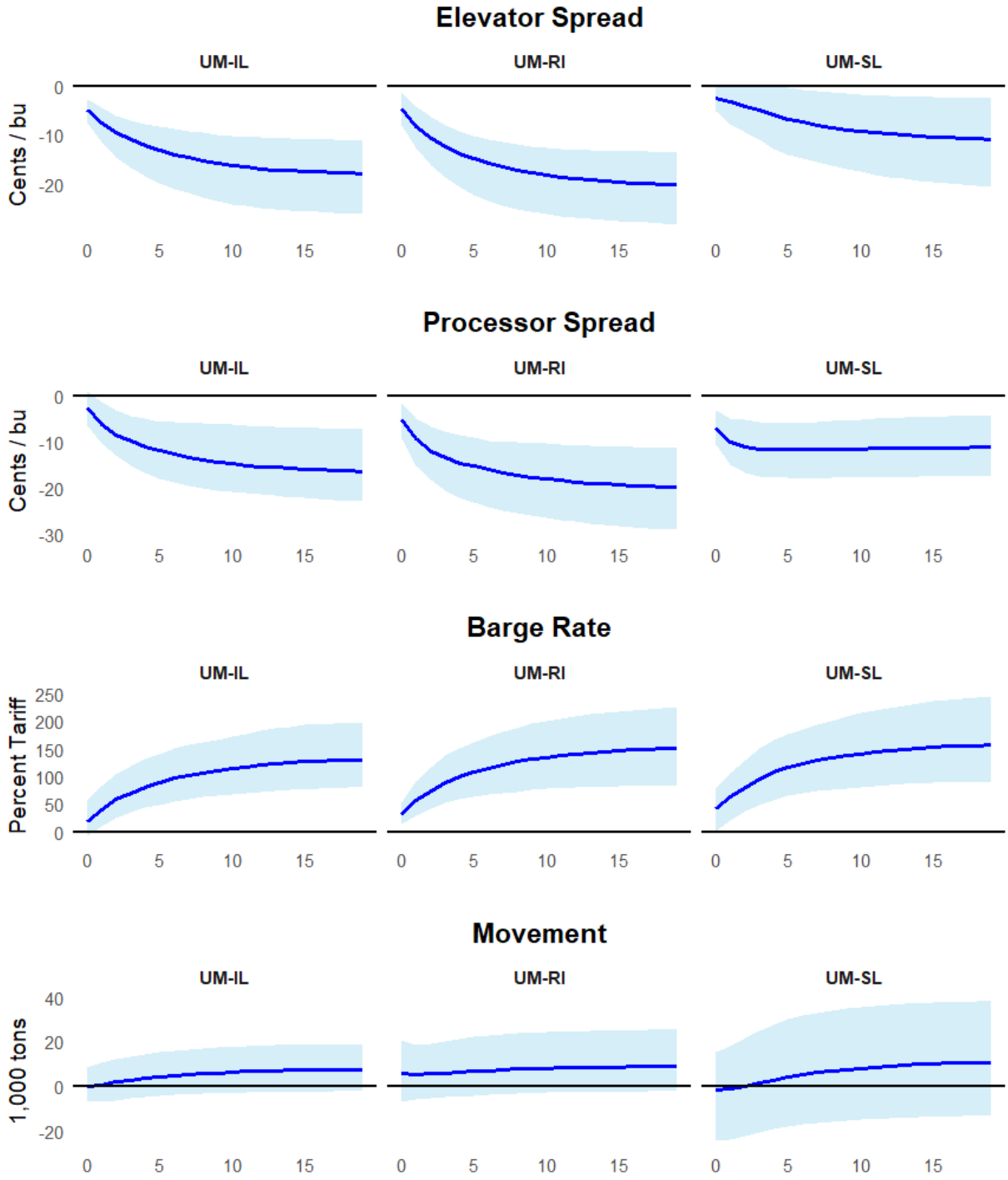
Appendix E. Robustness Check – Winter

Figure E1. Impulse Responses of Drought Shock with Winter Robustness Check 1: Corn



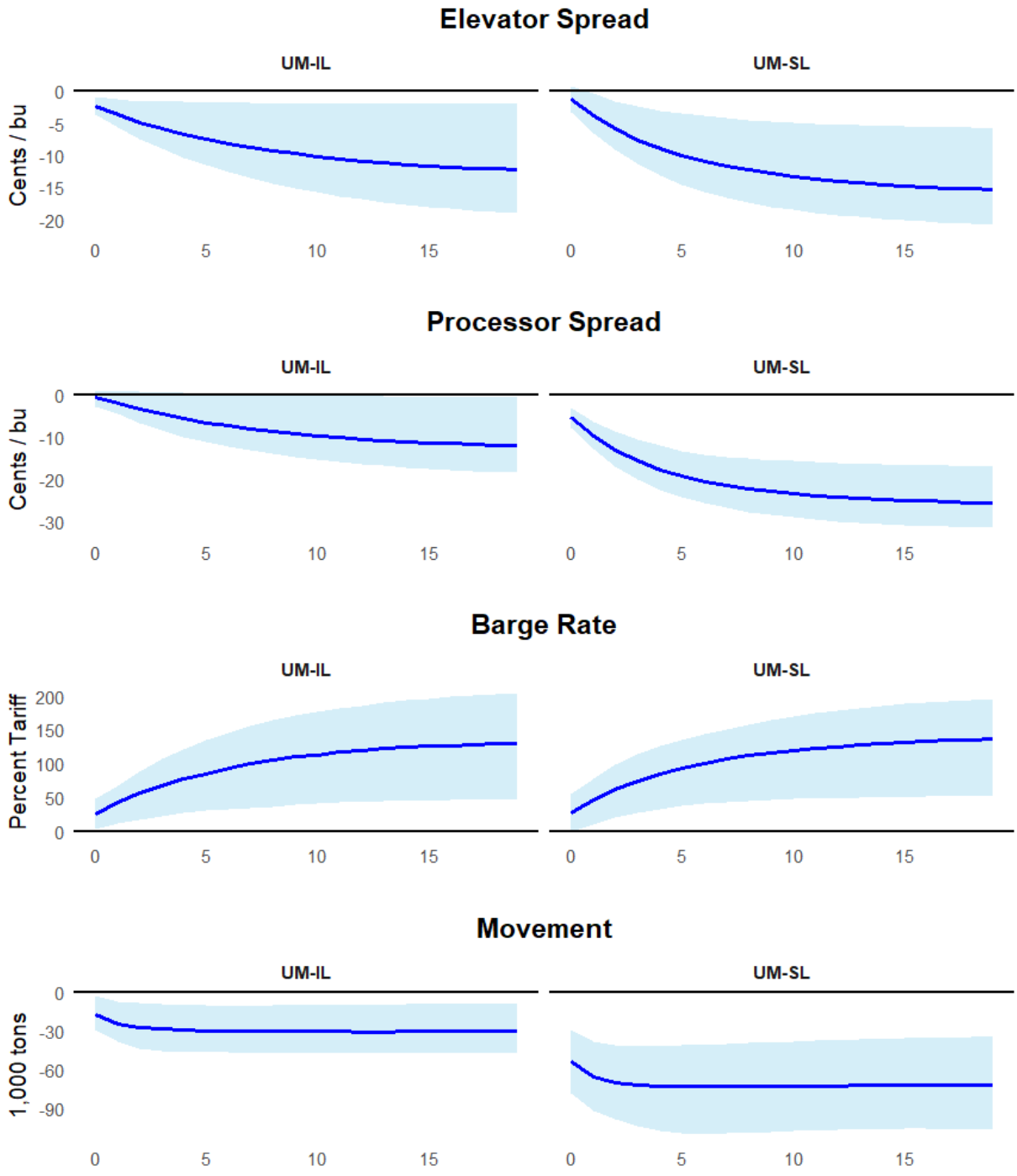
Note: Winter Robustness check 1 with imputed winter variables. The figures report the generalized impulse response functions (GIRFs) to a low-water shock, defined as a 15-foot decline in the St. Louis river stage from its sample median. Shaded areas indicate 95% confidence intervals based on stratified bootstrap procedures. All responses are expressed as deviations from their baseline paths.

Figure E2. Impulse Responses of Drought Shock with Winter Robustness Check 1: Soybean



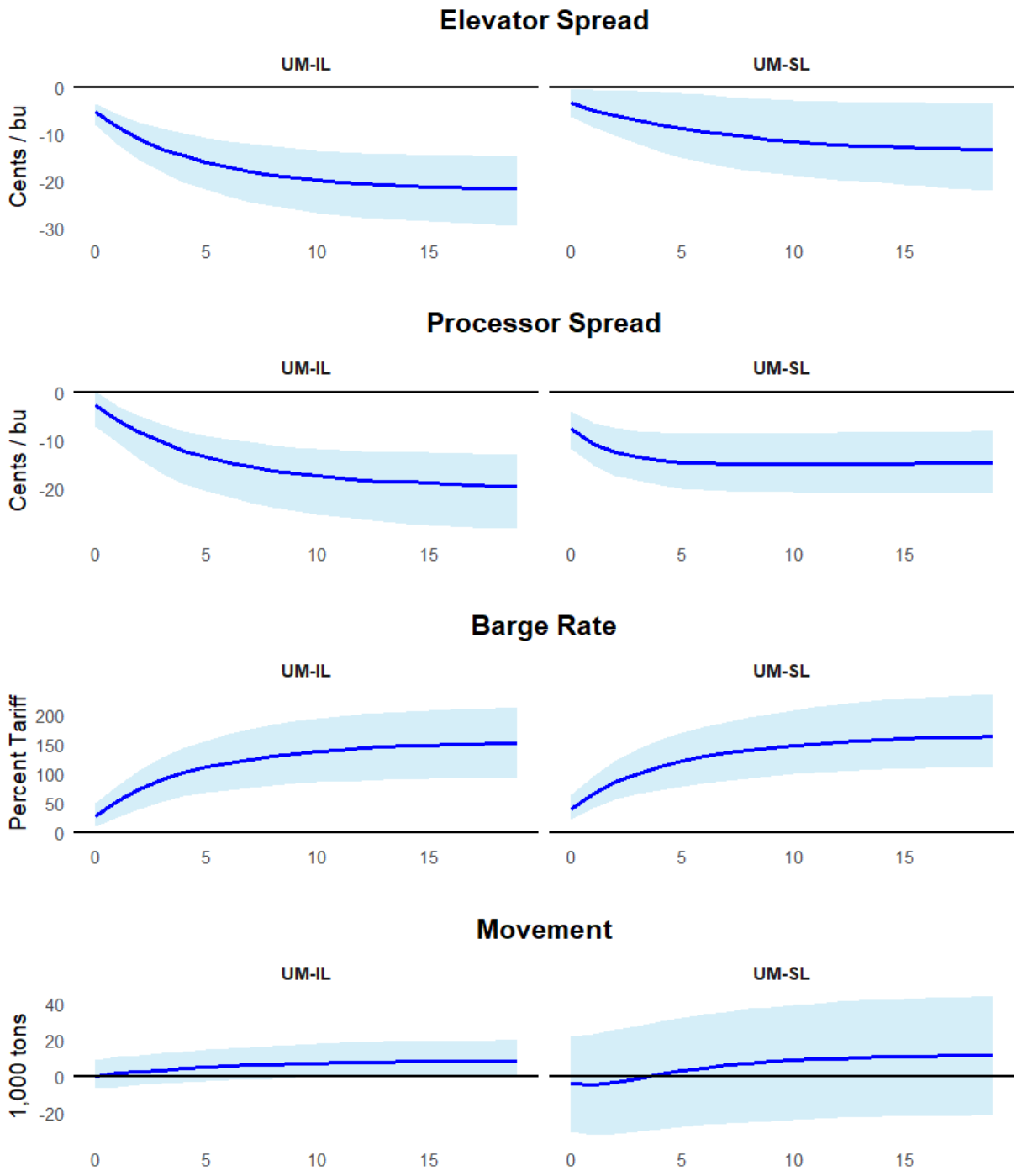
Note: Winter Robustness check 1 with imputed winter variables. The figures report the generalized impulse response functions (GIRFs) to a low-water shock, defined as a 15-foot decline in the St. Louis river stage from its sample median. Shaded areas indicate 95% confidence intervals based on stratified bootstrap procedures. All responses are expressed as deviations from their baseline paths.

Figure E3. Impulse Responses of Drought Shock with Winter Robustness Check 2: Corn



Note: Winter Robustness check 2 with winter retained and UM-RI excluded. The figures report the generalized impulse response functions (GIRFs) to a low-water shock, defined as a 15-foot decline in the St. Louis river stage from its sample median. Shaded areas indicate 95% confidence intervals based on stratified bootstrap procedures. All responses are expressed as deviations from their baseline paths.

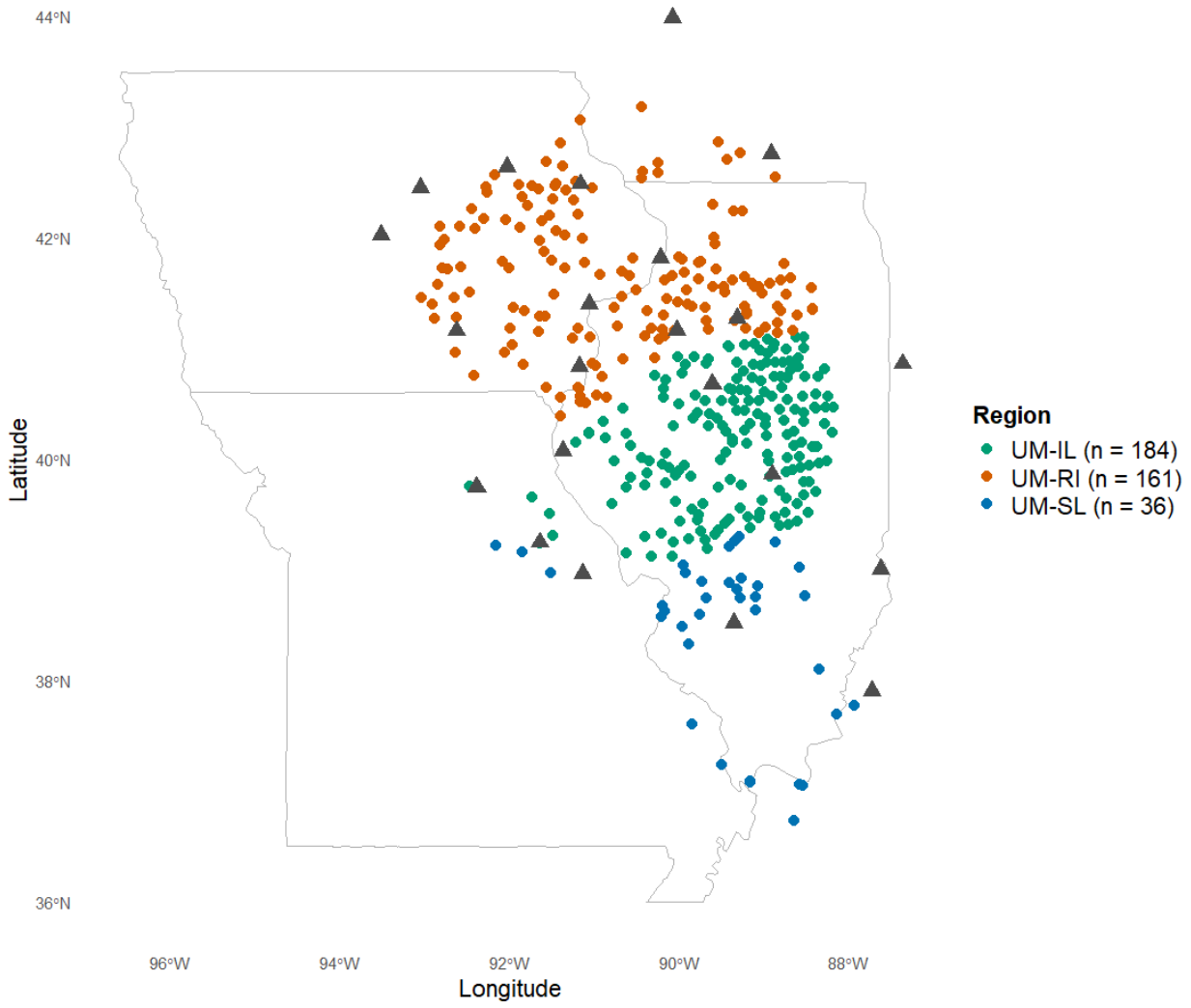
Figure E4. Impulse Responses of Drought Shock Winter Robustness Check 2: Soybean



Note: Winter Robustness check 2 with winter retained and UM-RI excluded. The figures report the generalized impulse response functions (GIRFs) to a low-water shock, defined as a 15-foot decline in the St. Louis river stage from its sample median. Shaded areas indicate 95% confidence intervals based on stratified bootstrap procedures. All responses are expressed as deviations from their baseline paths.

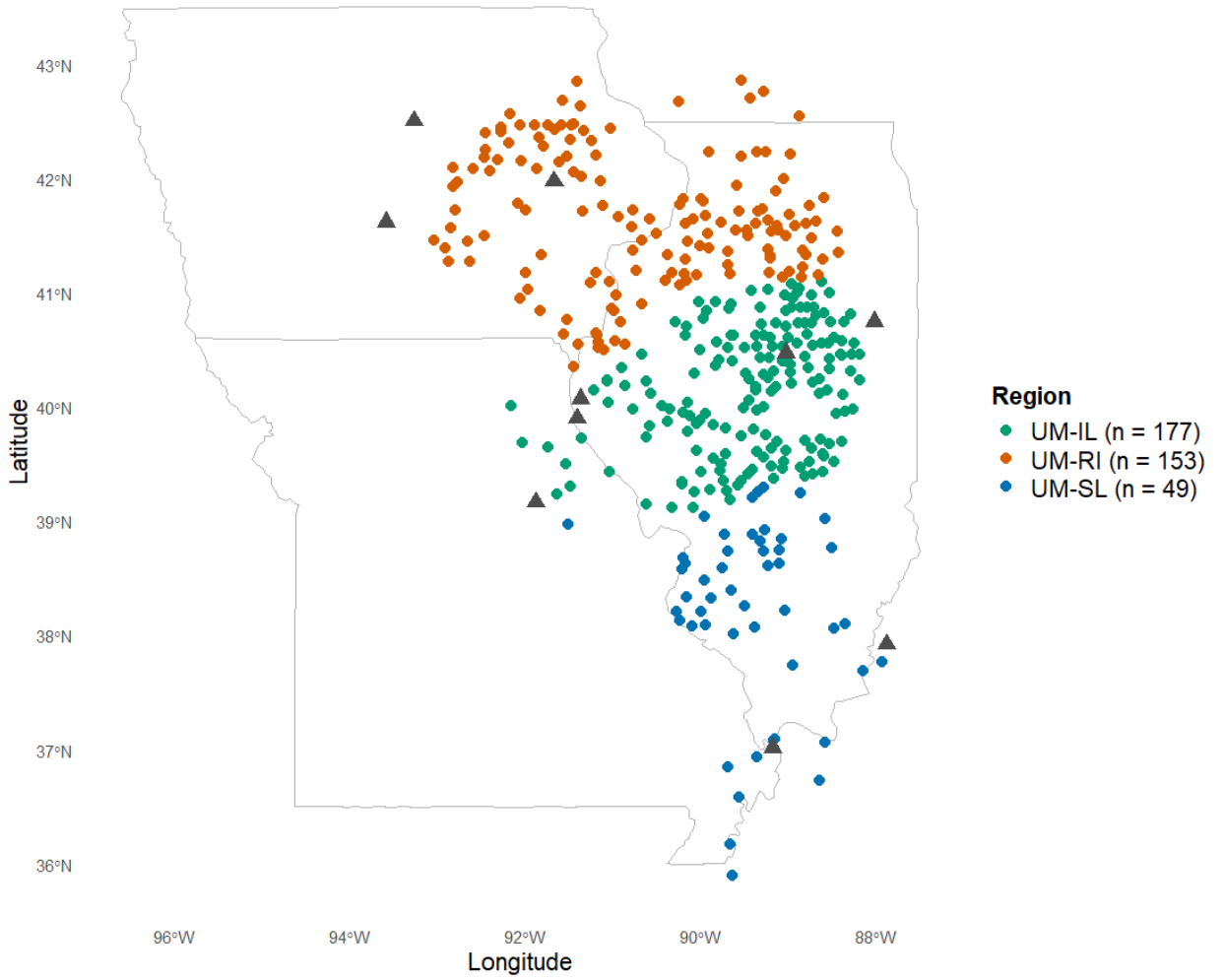
Appendix F. Robustness Check – Distance Identification

Figure F1. Corn Elevators and Processors Map Based on 100-Mile-Radius Identification



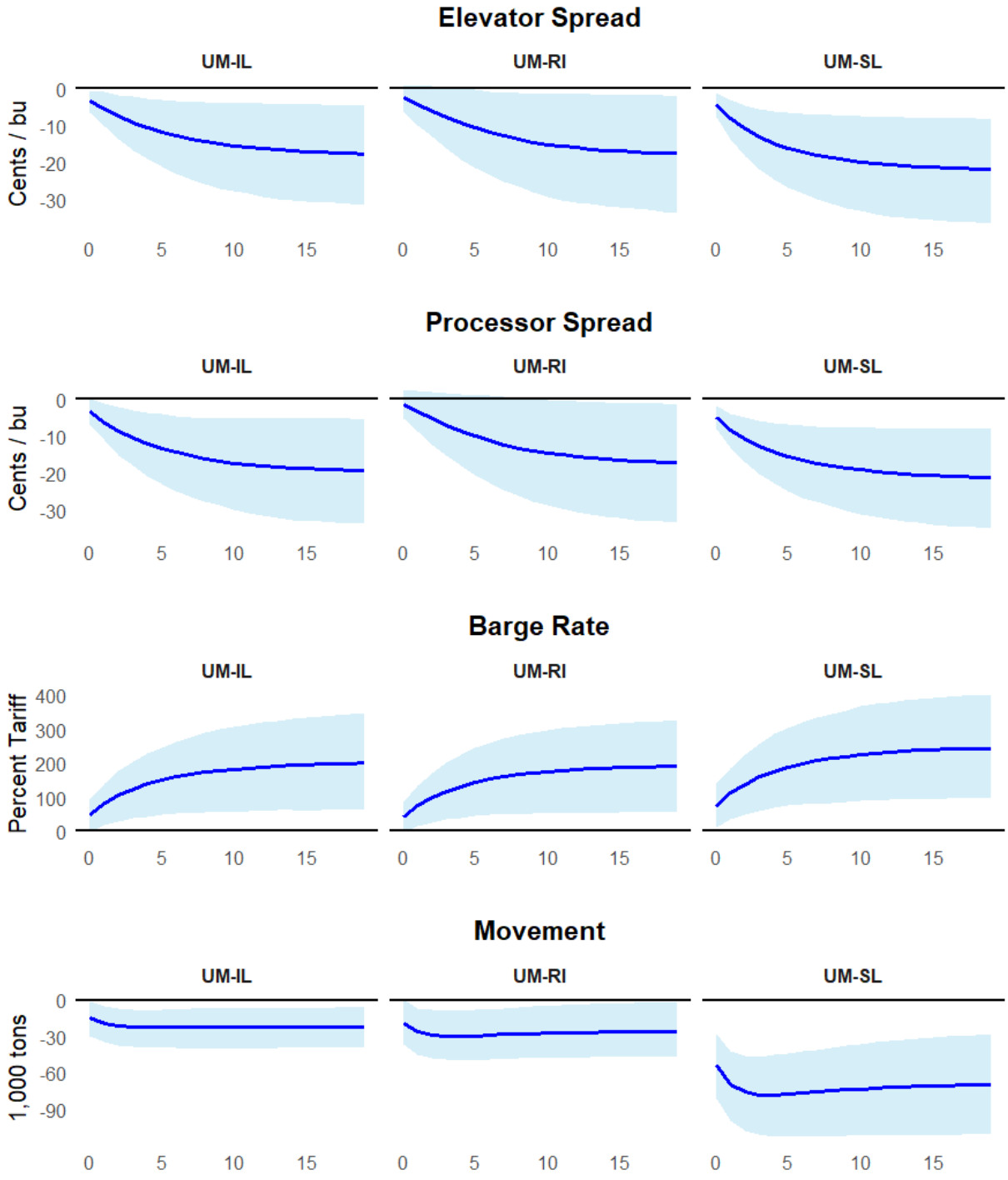
Note: This figure displays the distribution and number of corn elevators associated with each region with the distance of identification to be 100 miles, marked as dots. The triangles represent corn processors. The processors could be included in two different regions.

Figure F2. Soybean Elevators and Processors Map Based on 100-Mile-Radius Identification



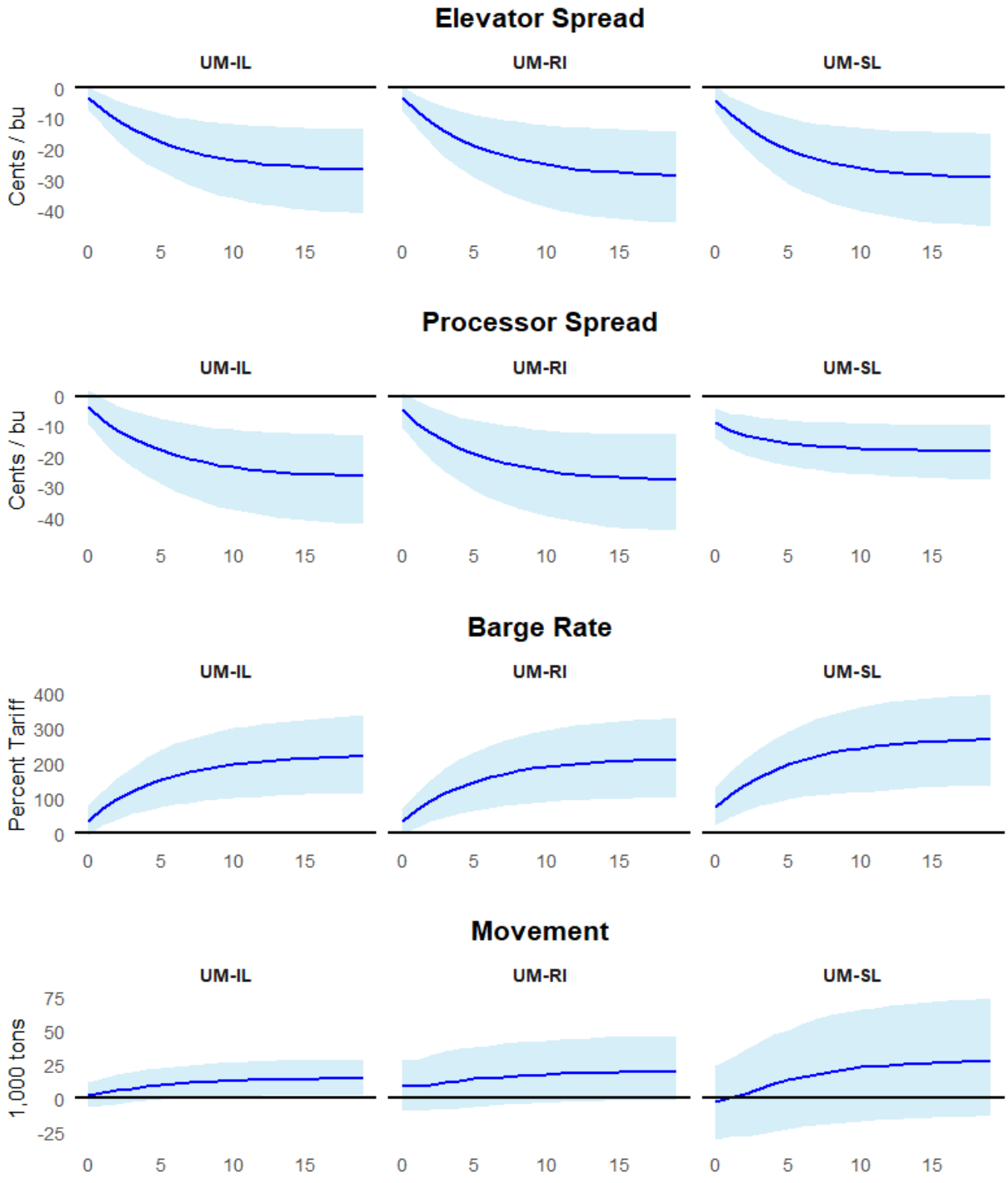
Note: This figure displays the distribution and number of soybean elevators associated with each region with the distance of identification to be 100 miles, marked as dots. The triangles represent soybean processors. The processors could be included in two different regions.

Figure F3. Impulse Responses of Drought Shock with Distance Robustness Check: Corn



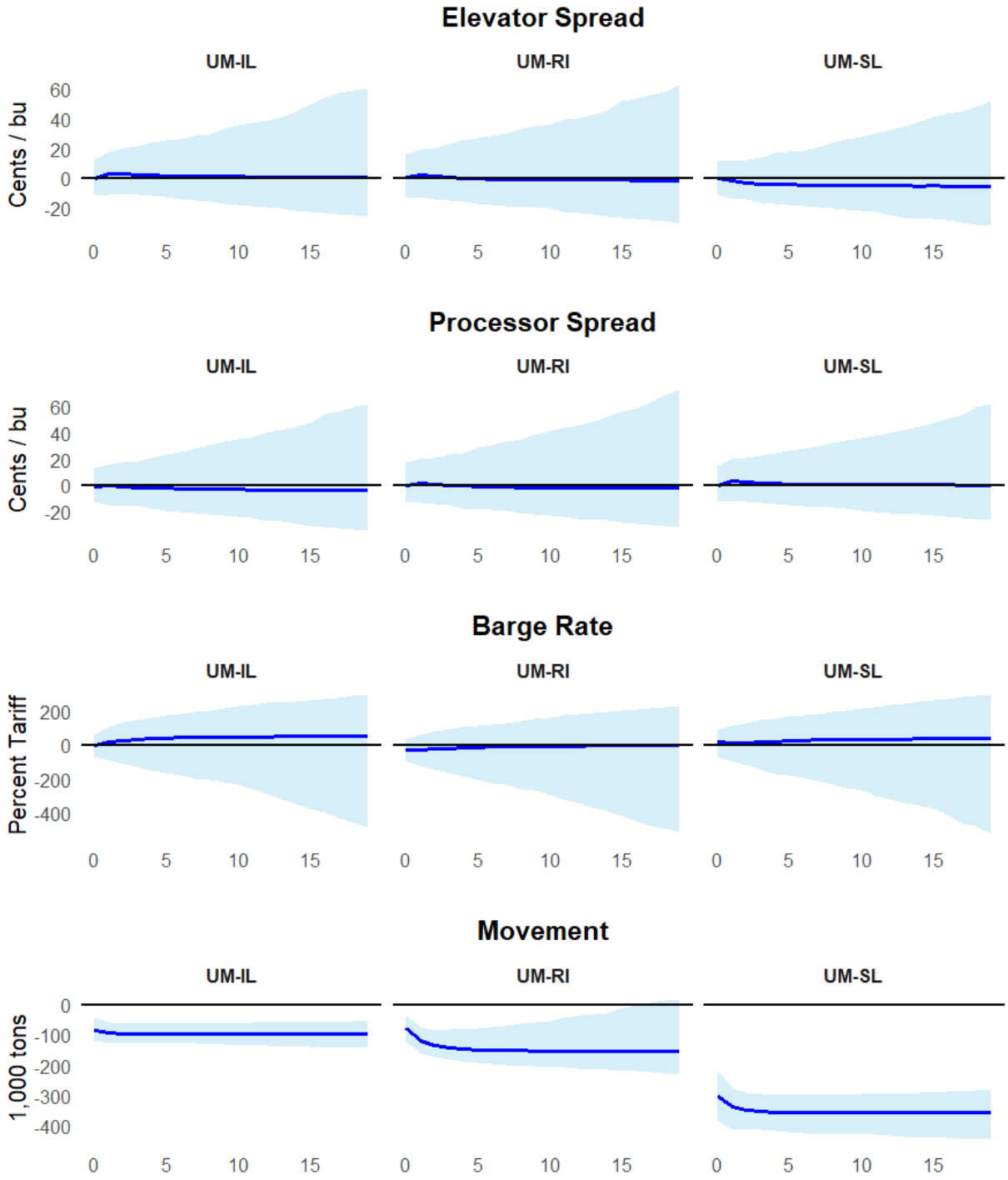
Note: Distance robustness check. The figures report the generalized impulse response functions (GIRFs) to a low-water shock, defined as a 15-foot decline in the St. Louis river stage from its sample median. Shaded areas indicate 95% confidence intervals based on stratified bootstrap procedures. All responses are expressed as deviations from their baseline paths.

Figure F4. Impulse Responses of Drought Shock with Distance Robustness Check: Soybean



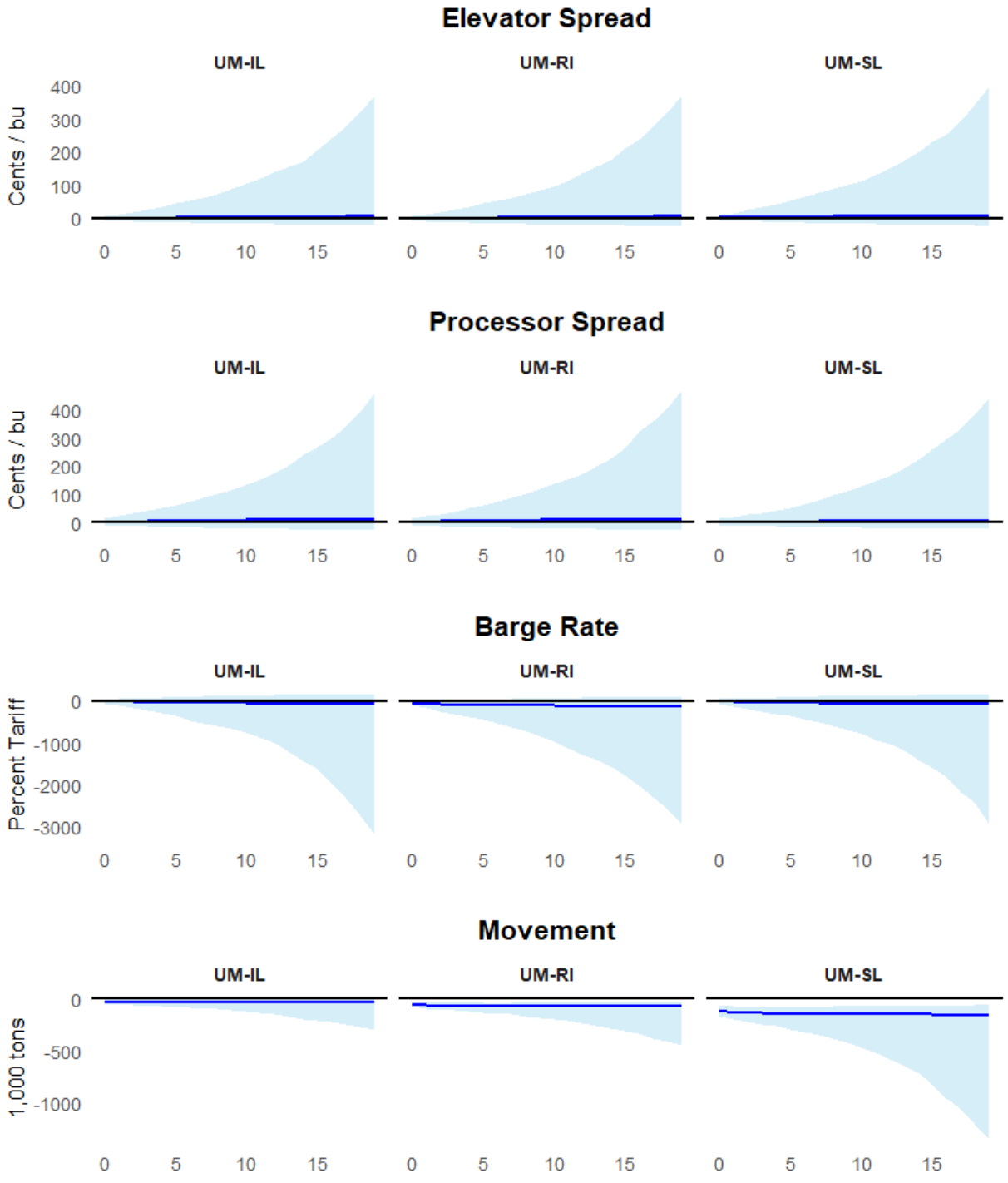
Note: Distance Robustness check. The figures report the generalized impulse response functions (GIRFs) to a low-water shock, defined as a 15-foot decline in the St. Louis river stage from its sample median. Shaded areas indicate 95% confidence intervals based on stratified bootstrap procedures. All responses are expressed as deviations from their baseline paths.

Figure F5. Impulse Responses of Flood Shock with Distance Robustness Check: Corn



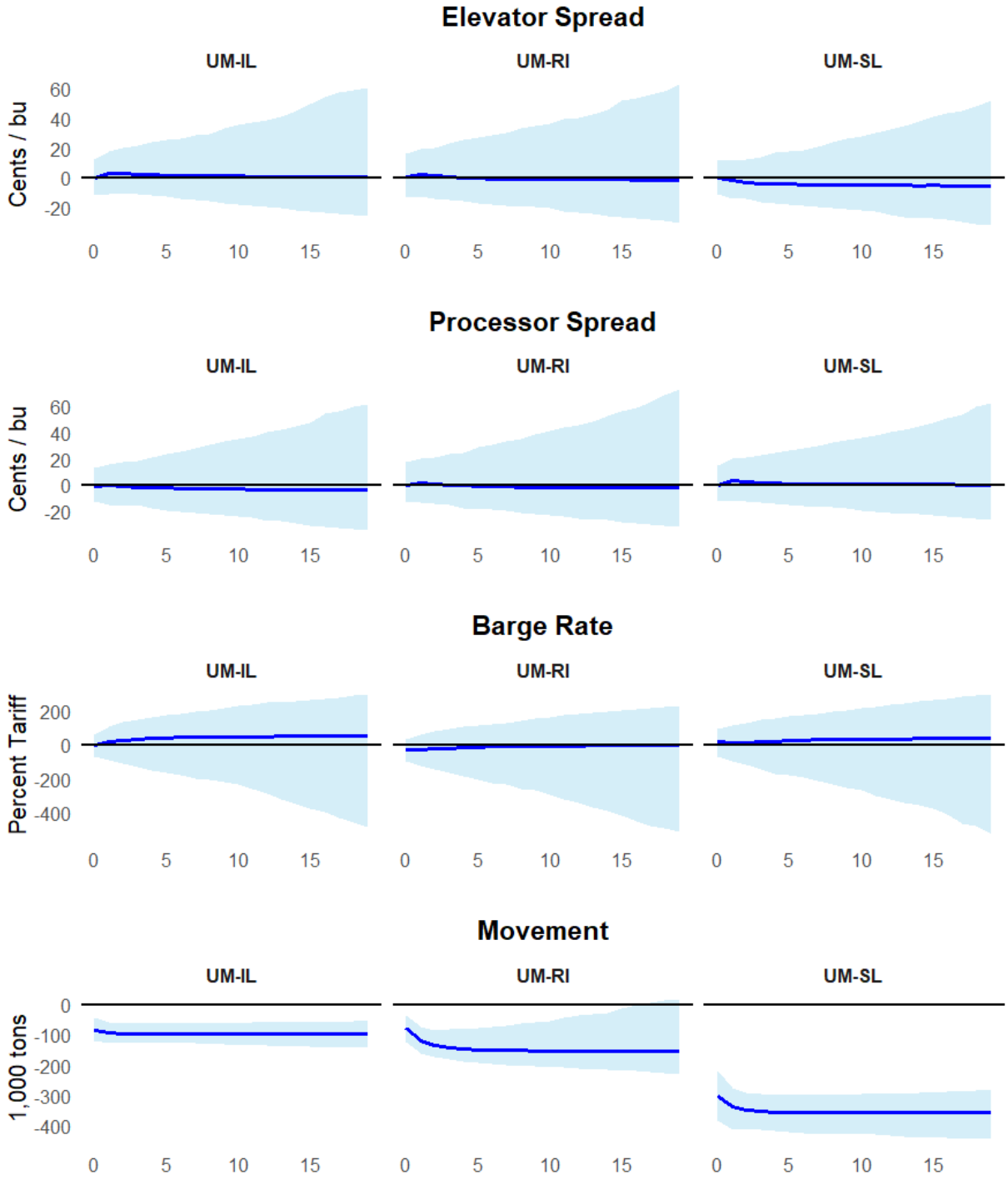
Note: Distance Robustness check. The figures report the generalized impulse response functions (GIRFs) to a high-water shock, defined as an increase of river stage in the St. Louis river stage from its sample median to 40 feet. Shaded areas indicate 95% confidence intervals based on stratified bootstrap procedures. All responses are expressed as deviations from their baseline paths.

Figure F6. Impulse Responses of Flood Shock with Distance Robustness Check: Soybean



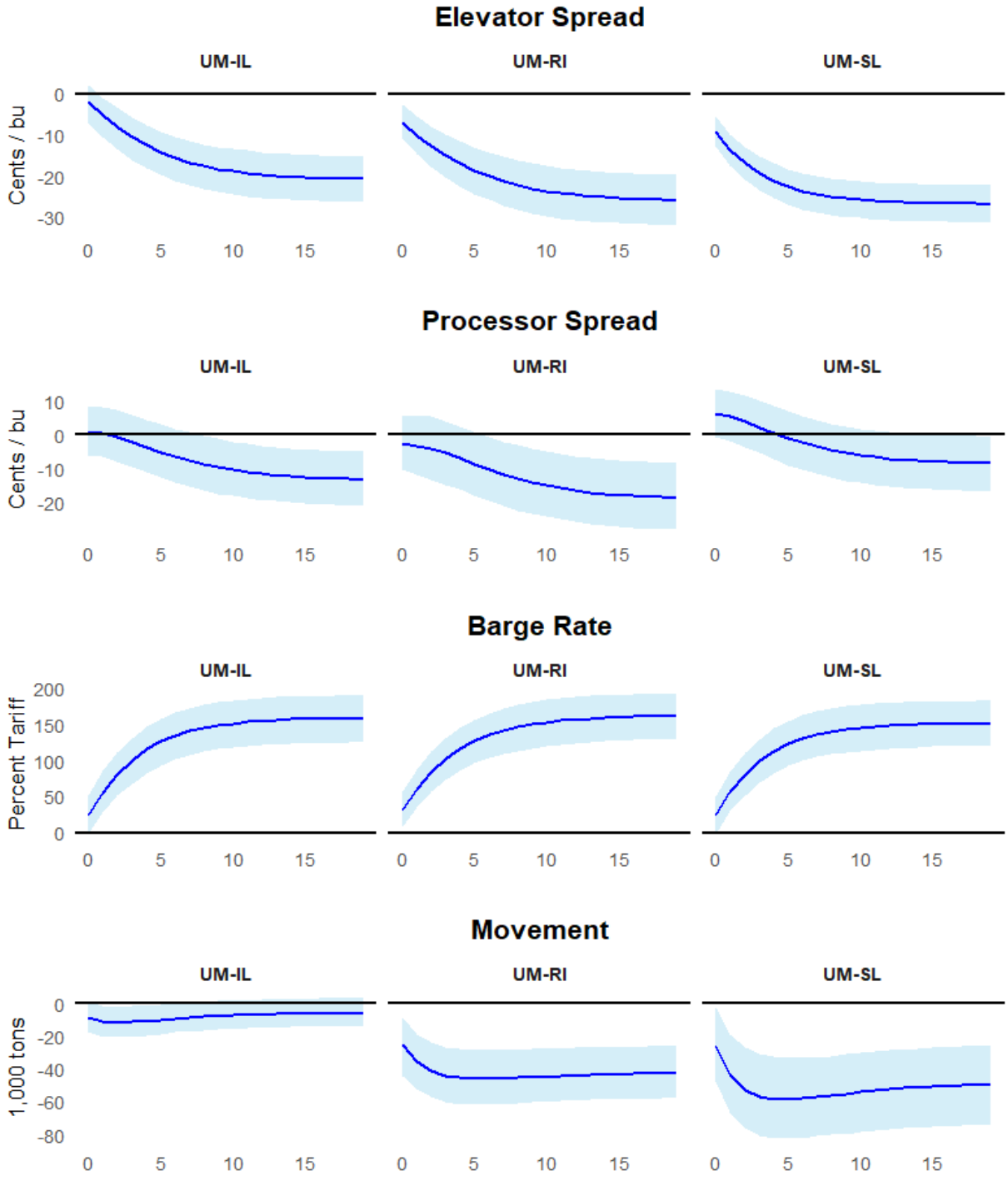
Note: Distance Robustness check. The figures report the generalized impulse response functions (GIRFs) to a high-water shock, defined as an increase of river stage in the St. Louis river stage from its sample median to 40 feet. Shaded areas indicate 95% confidence intervals based on stratified bootstrap procedures. All responses are expressed as deviations from their baseline paths.

Figure F7. Impulse Responses of Energy Shock with Distance Robustness Check: Corn



Note: Distance Robustness check. The figures report the generalized impulse response functions (GIRFs) to an energy shock, defined as the Midwest diesel price from its sample median to $5 per gallon. Shaded areas indicate 95% confidence intervals based on stratified bootstrap procedures. All responses are expressed as deviations from their baseline paths

Figure F8. Impulse Responses of Energy Shock with Distance Robustness Check: Soybean



Note: Distance Robustness check. The figures report the generalized impulse response functions (GIRFs) to an energy shock, defined as the Midwest diesel price from its sample median to $5 per gallon. Shaded areas indicate 95% confidence intervals based on stratified bootstrap procedures. All responses are expressed as deviations from their baseline paths